

Supplementary Information for

Sequence-encoded and Composition-dependent Protein-RNA Interactions Control Multiphasic Condensate Topologies

Taranpreet Kaur^a, Muralikrishna Raju^{b§}, Ibraheem Alshareedah^{a§}, Richoo B. Davis^a, Davit A. Potoyan^{*b}, Priya R. Banerjee^{*a}

^aDepartment of Physics, University at Buffalo, Buffalo NY 14260, USA

^bDepartment of Chemistry, Iowa State University, Ames IA 50011, USA

§These authors contributed equally

*Corresponding Authors:

Priya R. Banerjee: prbanerj@buffalo.edu

Davit A. Potoyan: potoyan@iastate.edu

Materials and Methods

Protein expression and purification: A list of the proteins used in this study is shown in Table S1. Codon optimized proteins of interest were gene-synthesized by GenScript USA Inc. (Piscataway, NJ, USA). The plasmid vector was a gift from Scott Gradia (Addgene plasmid # 29706). Proteins were expressed and purified using affinity chromatography as described in our earlier work with one modification¹. Cells were lysed using a sonicator for 2 minutes (Branson Digital Sonifier 450, 3 mm tapered microtip, 50% amplitude, 10 s ON/ 50 s OFF) in an ice bath.

Fluorescence labeling: The cysteine-containing variants of the proteins were gene synthesized by GenScript USA Inc. (Piscataway, NJ, USA) through site-directed mutagenesis. The proteins were expressed and purified using an identical protocol as described above with one modification: all buffers contained 1 mM DTT to prevent cysteine cross-linking. The protein samples were fluorescently labeled with either Alexa488 dye, Alexa594 dye, or Cy5 dye (C5-maleimide derivative, Molecular Probes) as described in the manufacturer protocol. The His6-MBP-N10 tag was removed by the action of TEV protease (TEV:protein = 1:25 v/v) for 1 h at 30 °C. Ni-NTA beads (ThermoFisher Scientific; Cat# 88223) were used to separate the tag from the proteins. The cleaved proteins were diluted in 25 mM Tris HCl (pH 7.5), 125 mM NaCl (final concentration: 2-10 μ M) and stored as aliquots at -80 °C. The labeling efficiency for all samples was observed to be \geq 65% (UV-Vis absorption measurements). All peptides [purchased through GenScript USA Inc. (Piscataway, NJ, USA)] contained a C-terminal cysteine which was used for site-specific labeling with Alexa488 or Alexa594 dyes using the same protocol as described in our earlier work²⁻⁶. A list of the proteins used in this study is shown in Table S1.

Peptide and RNA stock preparation: All the peptides used ([RGRGG]₅, [KGKGG]₅, [KGYGG]₅, RGG-3 domain of FUS) were purchased from Genscript USA Inc. (NJ, USA). All peptides contained a C-terminus cysteine for site-specific peptide labeling. Peptide stock solutions were prepared in RNase-free water (Santa Cruz Biotechnology) with 50 mM dithiothreitol (DTT). Polyuridylic acid [poly(U); Sigma-Aldrich; molecular weight = 600-1000 kDa], Polyadenylic acid [poly(A); Sigma-Aldrich; molecular weight =100-500 kDa] and custom-synthesized RNA oligos poly(rU)-U40 [40 nucleobases; Integrated DNA Technologies (IDT); molecular weight =12185 Da] were reconstituted in RNase-free water. The concentration of all RNAs was calculated from their respective measured absorbance at 260 nm in a UV-Vis spectrophotometer (Nanodrop oneC). Both RNA and peptide stock solutions were stored at -20 °C. Before sample preparation for experiments, the RNA [poly(U), poly(A), and U40] stock solutions were checked for any aggregates using bright-field microscopy. Nucleic acid staining dye SYTO13 was purchased from Thermo Fisher Scientific Inc.

State diagram analyses: State diagrams for all FUS^{PLD}-peptide mixtures were determined using optical microscopy. Before sample preparation, FUS^{PLD} was buffer exchanged (to remove the glycerol used in the storage buffer) into 25 mM Tris-HCl buffer (pH 7.5) at room temperature. This is followed by the removal of His6-MBP-N10 tag using TEV protease (TEV:protein = 1:25 v/v) in a 25 mM Tris HCl (pH 7.5) buffer containing 150 mM NaCl for 1 hr at 30 °C. Samples for phase diagram analyses were prepared at room temperature at the desired FUS^{PLD} and peptide concentrations in a 25 mM Tris-HCl buffer containing 150 mM NaCl and 20 mM DTT (pH 7.5). Samples were then placed onto a Tween20-coated (20% vol/vol) microscope glass slide and loaded under a Zeiss Primo-vert inverted iLED microscope (40x or 100x objective). Images were captured using a built-in Zeiss Axiocam 503 monochrome camera. Samples were kept covered with a glass cover to prevent concentration fluctuations due to evaporation and monitored for 2-5 minutes for droplet formation. The mixture was marked as LLPS or no LLPS depending on the clear existence of visible droplets throughout the microscopic field of view. The state diagram for FUS^{PLD}-poly(U) mixtures was also obtained in a similar manner except the sample buffer used

was 25 mM Tris HCl (pH 7.5) buffer, 150 mM NaCl without any DTT. The samples for RLD-RNA state diagram were also prepared at room temperature in 25 mM Tris-HCl buffer containing 150 mM NaCl and 20 mM DTT (pH 7.5) and were analyzed for the existence of droplets in a similar manner as stated above.

Apparent diffusion coefficient measurement using FRAP: Zeiss LSM710 laser scanning confocal microscope with a 63x oil-immersion objective (Plan-Apochromat 63x/1.4 oil DIC M27) was used for fluorescence recovery after photobleaching (FRAP) experiments. Phase-separated FUS^{PLD}-peptide samples were prepared at a fixed FUS^{PLD} concentration (280 μ M) and varying peptide concentration in a buffer containing 25 mM Tris-HCl, 150 mM NaCl, and 20 mM DTT (pH 7.5). These samples correspond to the FUS^{PLD} concentrations above the homotypic phase-separation threshold for FUS^{PLD} as shown in the FUS^{PLD}-peptide state diagrams (Figs. 1a&5a in the main-text). Sample preparation of FUS^{PLD}-peptide mixtures for FRAP was done in a similar manner as described above for the state diagram analyses except for the addition of fluorescent probes. Approximately 1% (labeled-to-unlabeled ratio) of Alexa488-labeled FUS^{PLD} (excitation/emission wavelengths; 488/ 503-549 nm) and Alexa594-labeled peptides (excitation/emission wavelengths; 595/ 602-632 nm) were used within the unlabeled protein-peptide mixtures. Samples were then placed inside a Tween20-coated (20% vol/vol) Nunc Lab-Tek Chambered Coverglass (ThermoFisher Scientific Inc.) for imaging and FRAP assays. For FRAP experiments, a circular region of interest was bleached with 100% power for ~2-6 seconds which was followed by an imaging scan for 300 s. The recorded Alexa488-labeled FUS^{PLD} intensity values from the bleached ROI were then corrected for photofading, normalized, and fitted with a 2D diffusion model to obtain the recovery half time $\tau_{1/2}$ as described in our earlier work¹. The apparent diffusion coefficient (D) was calculated using the formula⁷

$$D = \frac{R^2}{4\tau_{1/2}}$$

Where R is the radius of the bleaching ROI (Figs. S2&17). The apparent diffusion coefficient was averaged for several samples (see statistical analysis section). Interval dot plots were plotted for comparison of apparent diffusion coefficients of FUS^{PLD} within FUS^{PLD}-peptide condensates at different peptide concentrations.

Partition coefficient measurements: Images for partition analysis were collected using the same instrument as for the FRAP measurements above. The same samples were used for FUS^{PLD}-peptide mixtures as described above in the FRAP section. All the confocal images were collected within 30 minutes of sample preparation. The partition coefficient (k) was calculated by dividing the mean intensity of Alexa488-labeled FUS^{PLD} per unit area inside the droplet by the mean intensity per unit area in the external dilute phase ($k = \frac{I_{in}}{I_{out}}$).

Client recruitment assay: Phase separated samples were prepared at a fixed concentration (1.0 mg/ml) of the peptide (FUS^{RGG3} or [KGKGG]₅) and variable concentrations of poly(U) RNA as mentioned in the text or the figure legends. The concentrations of poly(U) RNA were chosen such that the RNA-to-peptide ratio maps the left, right, and peak points on the turbidity plots of respective peptide and RNA (Fig. S15). To measure the recruitment of different clients in peptide-poly(U) droplets, ~500 nM of Alexa-488 labeled clients (FUS^{PLD}; EWSR1^{PLD}; Pol II CTD; BRG1^{LCD}; FUS^{FL}) were added to the sample mixture (Fig. 1g-k, main-text). The sample also contained 1% (labeled:unlabeled ratio) of Alexa594-labeled peptides for visualization of the condensates. The samples were prepared in 25 mM Tris-HCL (pH 7.5), 150 mM NaCl, and 20 mM DTT buffer. The order of addition of different components during sample preparation was buffer, peptide, client, and poly(U). The sample was placed inside a Tween20-coated (20% vol/vol) 8-well Nunc Lab-

Tek chambered coverglass and images were collected using Zeiss LSM710 laser scanning confocal microscope with 63x oil-immersion objective (Plan-Apochromat 63x/1.4 oil DIC M27). The recruitment assays for BRG1^{LCD} and FUS^{FL} were collected using LUMICKSTM C-trap, 60x water-immersion objective wherein the sample was inserted in a Tween20-coated (20% vol/vol) 25 mm x 75 mm x 0.1 mm custom-made flow chamber. All the images were collected within 1 hour of sample preparation. The client recruitment was quantified using the client partition coefficient (k) within the peptide-RNA droplets. The partition coefficient (k) was calculated by dividing the mean intensity of Alexa 488-labeled client per unit area inside the droplet by the mean intensity per unit area in the external dilute phase ($k = \frac{I_{in}}{I_{out}}$).

RNA-mediated PLD-RLD condensate switching and demixing assays: FUS^{PLD}-RLD (RLD = FUS^{RGG3} or [RGRGG]₅) mixtures were prepared as described in the state diagram and the FRAP experiment sections. FUS^{PLD} and RLD concentrations were chosen within the green/pink region in the state diagram (Fig. 1a-main text; and Fig. S1) above and below the saturation concentration of FUS^{PLD} homotypic phase-separation in respective samples as described in the text. Samples were prepared in a buffer containing 25 mM Tris-HCl (pH 7.5), 150 mM NaCl, and 20 mM DTT and approximately 1% (labeled:unlabeled ratio) of Alexa 488-labeled FUS^{PLD} (Figs. 2 and 3a-c, main-text) and Alexa 594-labeled peptide were added for fluorescence microscopy. Each sample was placed inside the Tween20-coated Nunc Lab-Tek chambered coverglass and loaded onto a Zeiss LSM710 laser scanning confocal microscope. The objective was focused at a suitable position in the middle of the sample with droplets. The Zeiss software was set to acquire time-lapse images continuously every 1.6 seconds before RNA addition. Once imaging is started, a 0.7-1 μ l drop of RNA [poly(U) or poly(A)] stock solution was added to the sample using a pipette far from the image acquisition spot to a final concentration of 2.5 or 5 times (as mentioned in the appropriate figure legends) that of RLD concentration in the sample (wt/wt). Time-lapse images were acquired until the droplets equilibrated after RNA addition. A control experiment with an identical volume of buffer addition instead of RNA addition was performed to ascertain that the changes seen in the FUS^{PLD}-RLD droplets were not due to concentration fluctuations (Fig S11). Time-lapse images for the control experiment were captured using a Zeiss Axiocam 503 monochrome camera mounted on a Zeiss Primo-vert inverted iLED microscope (40x objective).

Preparation and imaging of multiphasic condensates: Before sample preparation, all the proteins were buffer exchanged to remove the glycerol present in the storage buffer. FUS^{PLD} was buffer exchanged in the same way as mentioned in the state-diagram analyses section while full-length FUS was buffer exchanged into a buffer constituting 25 mM Tris-HCl (pH 7.5) and 150 mM NaCl (pH 7.5). Next, the His6-MBP-N10 tag was cleaved using TEV protease (1:25 volume ratio-TEV:protein) for 1 h at 30 °C. Homotypic FUS^{PLD}/ FUS^{FL} droplets were formed at room temperature at concentrations (FUS^{PLD} = 400-500 μ M; or FUS^{FL} = 21 μ M) well above their respective homotypic phase-separation thresholds¹. 1-2 % of the labeled protein was added to the sample of unlabeled proteins. For the fluorescent labels, we used Alexa488-labeled (Figures: 3e, 4b and 5c&g, main-text) or Cy5-labeled (Figures: 3h and 5f, main-text) FUS^{PLD} as well as Alexa488-labeled FUS^{FL}. In some instances, FUS^{PLD} was used to visualize FUS condensates (Fig. 5f&g, main-text). The fluorescent probes for the supplementary figures are indicated in the appropriate figure legends. In parallel to this, peptide-RNA droplets were prepared in a separate tube with a fixed concentration of the peptide (as mentioned in respective figure legends) and variable concentration of poly(U) RNA. The concentrations of poly(U) RNA were chosen such that poly(U)-to-peptide ratios map the left, right, and peak points on the turbidity plots of respective peptide and poly(U) mixtures (Fig. S15). Approximately 500 nM of Alexa594-labeled peptides were used for fluorescence imaging. The buffer used for the samples contained 25 mM Tris-HCl, 150 mM NaCl and 20 mM DTT (pH 7.5). These preformed peptide-RNA droplet samples were then mixed 1:1 (v/v) with homotypic FUS^{PLD}/ FUS^{FL} droplet samples. The resulting mixture

containing the two types of droplets was then placed at the center of a Tween20-coated (20% v/v) 25 mm × 75 mm × 1 mm glass slide. The sample was then sealed with an 18 mm square coverslip of 0.1 mm thickness using double-sided tape. The resulting protein and peptide-RNA droplet samples were imaged using a laser scanning confocal microscope (LUMICKS™ C-trap, 60x water-immersion objective). All the images were collected within one hour of sample preparation. The same method of preparation was used for U40 RNA-peptide multiphasic condensates (Fig. 3e).

Contact angle analysis: Contact angles between the co-existing PLD (FUS^{PLD}) droplets and RLD-RNA ([RGRGG]₅-poly(U) RNA) droplets for the various samples were measured manually using the Angle Tool in Fiji-ImageJ⁸. Three tangent lines were drawn; (a) a tangent at the PLD-solvent interface, (b) a tangent at the interface between RLD-RNA droplet and the solvent, and (c) a tangent at the interface between PLD droplets and RLD-RNA droplets. The angle between tangent (a) and tangent (c) was taken as the PLD contact angle (Θ_{PLD}). The angle between tangent (b) and tangent (c) was taken as the RLD contact angle (Θ_{RLD}). The contact angle values obtained from several condensates were averaged (see the statistical analysis section).

Turbidity measurements: FUS^{RGG3} and poly(U) mixtures were prepared at a fixed FUS^{RGG3} concentration and variable poly(U) concentrations in a buffer containing 25 mM Tris-HCl, 150 mM NaCl and 20 mM DTT (pH 7.5). Sample absorbance at 350 nm was measured using a spectrophotometer (Nanodrop oneC UV-Vis) with an optical path length of 1 mm. A gradual poly(U) titration was used to record the turbidity data.

Fluid interface simulation: To explore the effect of surface tension on multi-phase coexistence, we used a fluid interface modeling tool (Surface Evolver v2.70)⁹. Briefly, two volumes of distinct liquids are created. Each interface is given a specific value of interfacial tension (see Fig. 4d and Fig. 6, main-text). The algorithm minimizes the total surface energy of the system using the gradient descent method⁹. As a control, we simulated the interfacial evolution of a cube of liquid, the minimization resulted in the transformation of the cube to a sphere¹⁰ [the minimum surface tension geometry] (Fig. S16). Throughout the minimization steps, the volumes of the two liquids were kept constant.

Fluorescence correlation spectroscopy: Samples containing 50 nM of Alexa488-labeled PLD were injected into a Tween-coated (Tween20) 25 mm x 75 mm x 0.1 mm custom-made flow chamber and loaded onto the microscope stage (Lumicks, C-trap) equipped with a single-photon Avalanche photodiode (sAPD). Measurements of the photon arrival times were acquired at a 100 MHz sampling rate by performing a point scan in the sample away from the glass surface. The excitation power was kept at a minimum to avoid photobleaching of the fluorophores. Each point scan was curated over a 5 minutes' period. For each sample [PLD and PLD+poly(U)], five point scans were obtained and analyzed as follows. For each point scan, the autocorrelation function was calculated for different lag times using the pycorrelate python library (version 0.2.1, see documentation at <https://pypi.org/project/pycorrelate/#description>). Five autocorrelation curves were averaged for each sample and plotted for comparison.

Stability assay for multiphasic condensates: Before sample preparation, FUS^{PLD} was buffer exchanged in the same way as mentioned in the state-diagram analyses section. The co-existing droplet sample was prepared by mixing all the three components in a test tube (FUS^{PLD}, [RGRGG]₅, poly(U) RNA) at the concentrations mentioned in the appropriate figure legend (Fig S13). Approximately 500 nM of Alexa488-labeled FUS^{PLD} and Alexa594-labeled RLD were used for fluorescence microscopy. The order of addition during sample preparation was buffer, FUS^{PLD}, [RGRGG]₅, fluorescent probes, and poly(U) RNA. ~ 5 uL volume of prepared sample was placed inside the tween20-coated Nunc Lab-Tek Chambered Cover glass and imaged using the Zeiss LSM710 laser scanning confocal microscope. The sample was covered with 100-200 uL of

Fluorinert™ FC-770 (Sigma-Aldrich), which is a highly inert liquid and completely immiscible with water. FC-770 layer on the top of the sample helps in avoiding sample drying and preserving the sample for days.

Statistical analysis: A two-tailed t-test was used for statistical analysis. **** represents a p-value < 0.0001, *** represents a p-value between 0.0001 and 0.001 and no star represents a p-value > 0.05. The number of droplets (n) analyzed in various figures is mentioned below.

Figure 1b&c: $n \geq 60$ for partition and $n=3-6$ for diffusion coefficient. *Figure 1k:* $n \geq 100$ for EWS^{PLD} partition, $n \geq 50$ for FUS^{PLD} partition and $n \geq 75$ for BRG1^{LCD} partition. *Figure 4c:* $n=25-55$ for contact angle measurements of each droplet type (θ_{PLD} and θ_{RLD}). *Figure 5b:* $n \geq 60$ for partition and $n=2-4$ for diffusion coefficient measurements. All statistical measurements were done on the same sample for each distinct experimental condition.

Data processing software: Excel 2016 was used for partition calculations, MATLAB (R2018a) was used for FRAP analysis and statistical analysis. Fiji-ImageJ⁸ (version 1.52p) was used for image processing. OriginPro (2018b) was used for Graphing. Adobe Illustrator CC was used for the figure assembly and production.

Molecular dynamics simulation: In this study, we have employed a single residue/base resolution coarse-grained polyelectrolyte model for protein and RNA chains. For the amino acids, we employ the same coarse-grained parameters as have been employed by Dignon et al.¹¹ to study the phase behavior of intrinsically disordered proteins. The potential energy function contains bonded, electrostatic, and short-range pairwise interaction terms. Bonded interactions are modeled using a harmonic potential $k_r(r - r_0)^2$ with a spring constant $k_r = 10 \text{ kJ}/\text{\AA}^2$ and an equilibrium bond length of $r_0 = 3.8 \text{ \AA}$. Electrostatic interactions are modeled using a Coulombic term with Debye-Hückel electrostatic screening to account for salt concentration, having the functional form:

$$E_{ij}(r) = \frac{q_i q_j}{4\pi D r} \exp\left(-\frac{r}{\kappa}\right) \quad (1)$$

where κ is the Debye screening length and $D = 80$, is the dielectric constant of the solvent (water). We set the Debye screening length $\kappa = 0.1$, which corresponds to approximately 100 mM salt concentration at room temperature. The RNA chain is modeled as a one bead per nucleotide model compatible with the protein model with the only difference being the addition of harmonic angular term $k_\theta(\theta - \theta_0)^2$ to model the stiffness of the RNA chains, where spring constant $k_\theta = 1.0 \text{ kJ}$ and equilibrium angle $\theta_0 = 1.78 \text{ rads}$.

The initial system configurations were generated by placing the protein and RNA chains randomly in the simulation box at concentrations corresponding to the experimental conditions. The system was energy-minimized with an energy tolerance of 10^{-7} kJ/mole and force tolerance of $10^{-7} \text{ kJ/mole-\AA}$. The system was then equilibrated in the canonical constant Number of particles, Pressure and Temperature (NPT) ensemble at 298 K and 1 atm using the Nose-Hoover thermostat and barostat with a coupling time constant of 1 ps and 10 ps respectively. The equilibrated system was further simulated in the canonical NVT ensemble at 298 K using the Langevin thermostat with a friction coefficient of $\gamma = 0.01$. MD runs were performed on graphical processing units (GPUs) using the HOOMD-blue package v2.7.0^{12,13}. The equilibrium run was performed for 10 ns with a time step of 0.01 ps and the production run was performed for an additional 10 ns. The surface-recruitment simulations shown in Figures 1f (main-text) and S21 were performed in two stages. In the first stage, the condensates under low RNA and high RNA

conditions were generated using the procedure above. In the second stage, PLD chains were randomly placed in the simulation box and the system was then equilibrated in the constant NVT ensemble at 298 K for 10 ns.

Supplementary Tables

Protein/ polypeptide	N-terminal Tag	Purpose of the N-terminal Tag/ site-directed mutagenesis	Extinction Coefficient ($M^{-1}\cdot cm^{-1}$)
FUS	His6-MBP-N10	Purification	138230
PLD of FUS (FUS ^{PLD})	His6-MBP-N10	Purification	103600
FUS S86C	His6-MBP-N10	Purification/ Cys-maleimide conjugation used for site-specific protein labeling	138230
FUS ^{PLD} S86C	His6-MBP-N10	Purification/ Cys-maleimide conjugation used for site-specific protein labeling	103600
EWS ^{PLD} A2C	His6-MBP-N10	Purification/ Cys-maleimide conjugation used for site-specific protein labeling	122970
RNA Pol II ^{CTD} 2C	His6-MBP-N10	Purification/ Cys-maleimide conjugation used for site-specific protein labeling	112540
BRG1 ^{LCD} 2C	His6-MBP-N10	Purification/ Cys-maleimide conjugation used for site-specific protein labeling	80790

Table S1. List of the proteins used in the study. Also, see Table S2 for their amino acid sequences. The molar extinction coefficients were calculated using ProtParam¹⁴.

Protein/Peptide	Sequence
FUS ^{PLD} (PLD)	MASNDY T QQATQSY G AYPTQPGQ G YSQQSSQ P YGQQS Y SGYSQSTDTSG Y G QSS Y SSYGQSQNS Y GTQSTPQ G YGSTGG Y GSSQSSQSS Y GQQSS Y PG Y GQQ PAPSSTSGS Y GSSSQSS Y GQPQSGS Y SQQPS Y GGQQQS Y GQQQS Y NPPQ G Y GQQNQ Y NSSSGGGGGGGGG
EWS ^{PLD}	MASTD Y STYSQAAAQ G YSAYTAQPTQ G YAQT T QAYGQQS Y GT Y GQPTDV S Y TQAQT T AT Y GQTA Y ATS Y GQPPT G YTTPTAPQ A YSQP V Q Y GT G AYDTTTAT V TTTQAS Y AAQSA Y GTQPA Y PAYGQ Q PAATAP T RPQDGNKPTETSQPQSSTGG Y NQPSLG Y GQSN Y SPQVPGS Y PMQPV T APPS Y PPTS Y SSTQPTS Y DQSS Y SQ QNT Y GQPSS Y GQQSS Y GQQSS Y GQPPTS Y PPQTGS Y SQAPSQ Y SQQSS Y GQQS
RNA Pol II CTD	M Y SPTSPAYEP R SPGG Y TPQSPS Y SPTSPS Y SPTSPS Y SPTSPN Y SPTSPS Y SP TSPS Y SPTSPS Y SPTSPS Y SPTSPS Y SPTSPS Y SPTSPS Y SPTSPS Y SPTSPS Y S PTSPS Y SPTSPS Y SPTSPS Y SPTSPS Y SPTSPS Y SPTSPS Y SPTSPN Y SPTSPN Y TPTSPS Y SPTSPS Y SPTSPN Y TPTSPN Y SPTSPS Y SPTSPS Y SPTSPS
FUS ^{FL}	MASND Y TQQATQSY G AYPTQPGQ G YSQQSSQ P YGQQS Y SGYSQSTDTSG Y G QSS Y SSYGQSQNS Y GTQSTPQ G YGSTGG Y GSSQSSQSS Y GQQSS Y PG Y GQQ PAPSSTSGS Y GSSSQSS Y GQPQSGS Y SQQPS Y GGQQQS Y GQQQS Y NPPQ G Y GQQNQ Y NSSSGGGGGGGGGGN Y GQDQSSMSSGGGSGGG Y GNQDQSGG G GSGG Y GQQD R GG R GGSGGGGGGGGG Y NRSSGG Y EP R GGGG R GG R GGMGGSD R GGFNKFGG P RDQGS R HDSEQD N SDNNTIFVQGLGENVTIESVAD Y FKQIGIIKT N KTGQPMIN L Y T DR E TGK L KEATV S FD D PPSA K AIDW F DG K E F SG N PIK V S F AT R R A DF N RGGG N RGG R GGG P M R GG Y GGGGSGGGG R GG FP S GGGGGGGQ R AGDWK C PNPT C EN M FW R NE C NQ C AK P K D GP G GG P GG S HMGG N Y G DD R RRGG R GG Y DRGG Y RRGG D RRGG R GGG D RRGG F GG D RRGG F GP G K MDS R GE H R Q D R R ER P Y
BRG1 ^{LCD}	MSTDPPLGG T RP G SP G PG P SP G AM L GP S PG P SP G SA H SM M GP S PG P PS A GH I PT Q GP G Y P QDN M H Q M H K P ME S M H E K GM S DD P RY N Q M K G M G M R SG G HAG M GP P SP M D Q HS Q Y P S L GG S E H ASS P V P AS G PS S GP Q M S SG P GG A P LD G AD P Q A L G Q N R G PT P FN Q N Q L H Q L RA Q IM A Y K M L AR G Q P LP D HL Q MA V Q G K RP M PG M Q Q MP T LP P PS V S A T G PG P GP G PG P GP P APP N Y S R P H G M G GP N MP P PG S GV P PG M PG Q PP G PP K P W EP E GP M AN A APT S T P Q K L I PP Q PT G R PS P APP A V P PA S P V M P P Q T Q SP G Q P A Q PA
[RGRGG] ₅	RGRGG RGRGG RGRGG RGRGG RGRGGC
[KGKGG] ₅	KGKGG KGKGG KGKGG KGKGG KGKGGC
[KGYGG] ₅	KGYGG KGYGG KGYGG KGYGG KGYGGC
FUS ^{RGG3}	RRGG R GG Y DRGG Y RRGG D RRGG F RRGG R GG D RGC
Peptide/RNA	Sequences utilized in simulation
RLD (FUS ^{RGG3})	RRGG R GG Y DRGG Y RRGG D RRGG F RRGG R GG D RGC
RNA	[U] ₁₀₀
PLD polypeptide	MASND Y TQQATQSY G AYPTQPGQ G YSQQSSQ P YGQQS Y SGYSQSTDTSG Y G QSS Y SSYGQSQNS Y GTQSTPQ G YGSTGG Y GSSQSSQSS Y GQQSS Y PG Y GQQ PAPSSTSGS Y GSSSQSS Y GQPQSGS Y SQQPS Y GGQQQS Y GQQQS Y NPPQ G Y GQQNQ Y NSSSGGGGGGGGG
FUS polypeptide	MASND Y TQQATQSY G AYPTQPGQ G YSQQSSQ P YGQQS Y SGYSQSTDTSG Y G QSS Y SSYGQSQNS Y GTQSTPQ G YGSTGG Y GSSQSSQSS Y GQQSS Y PG Y GQQ PAPSSTSGS Y GSSSQSS Y GQPQSGS Y SQQPS Y GGQQQS Y GQQQS Y NPPQ G Y GQQNQ Y NSSSGGGGGGGGG RR GG R GG Y DRGG Y RRGG D RRGG F RRGG R GG G D RGC

Table S2. Amino acid sequences of the proteins and peptides used in the study. Highlighted residues are Tyrosine (red) and Arginine (blue) residues.

Supplementary Figures

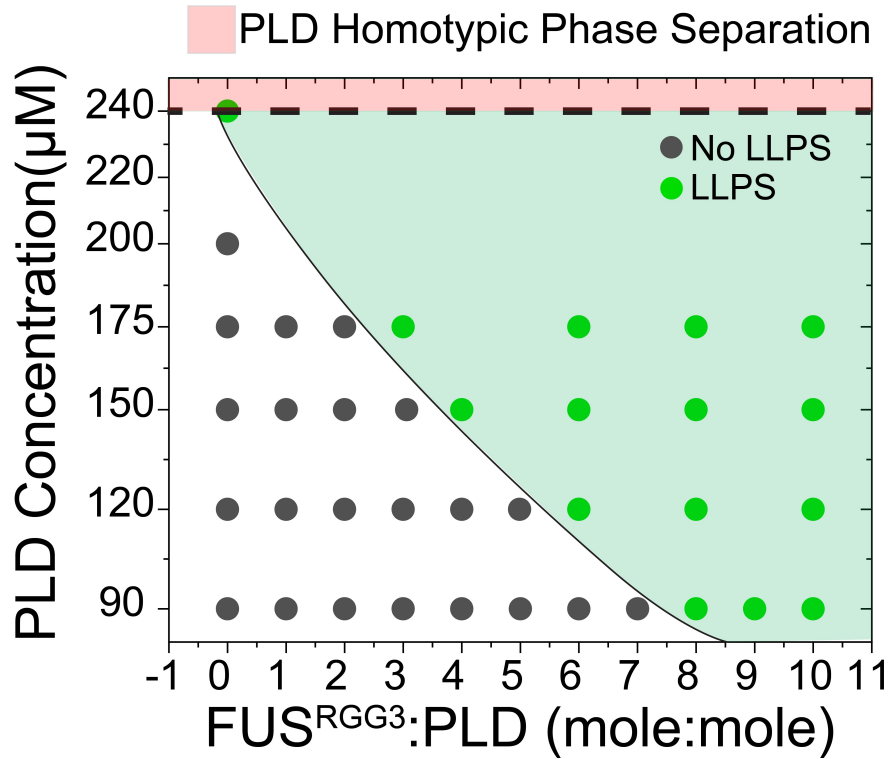


Figure S1. FUS^{RGG3}-PLD isothermal state diagram. State diagram for PLD-FUS^{RGG3} mixtures, showing that FUS^{RGG3} facilitates PLD (FUS^{PLD}) phase separation. Shaded green region shows co-phase separation regime for PLD-FUS^{RGG3} mixtures while the shaded pink region denotes PLD homotypic phase separation regime (saturation concentration ~240 μM). Both shaded regions are drawn as a guide to the eye. The sample buffer contains 25 mM Tris-HCl (pH 7.5), 150 mM NaCl and 20 mM DTT.

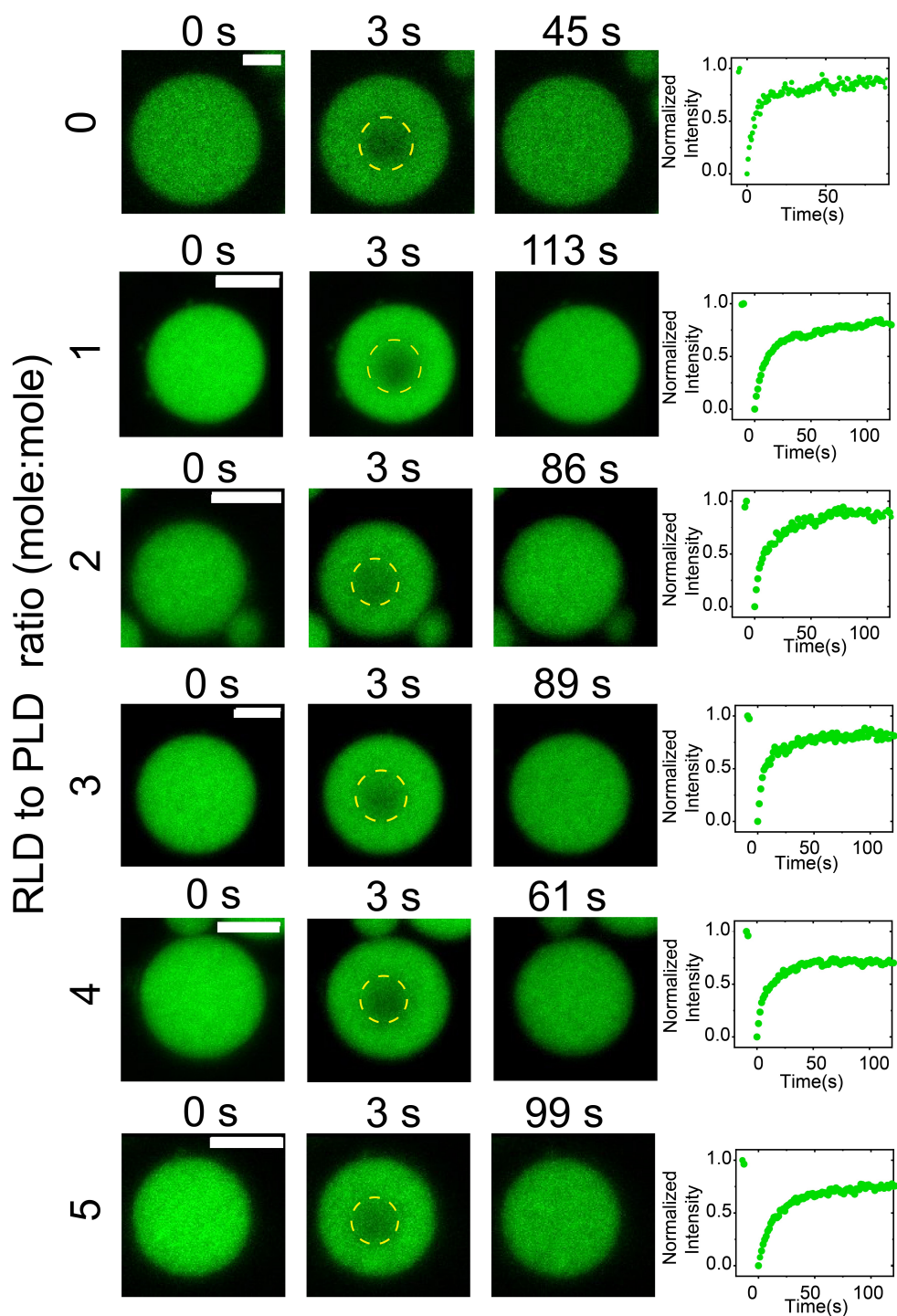


Figure S2. Representative experimental data for FRAP experiments on PLD-RLD condensates. Time-lapse FRAP images (left) and the corresponding intensity time traces (right) for PLD-RLD condensates prepared at a fixed FUS^{PLD} concentration of 280 μM and variable [RGRGG]₅-to-FUS^{PLD} ratios. The sample buffer contains 25 mM Tris-HCl (pH 7.5), 150 mM NaCl and 20 mM DTT. The yellow dashed circle indicates the predetermined bleaching region. Scale bars are 5 μm. Bleaching occurs at t=3s. The FRAP experiment was performed utilizing ~1% (labeled:unlabeled ratio) Alexa488-labeled PLD.

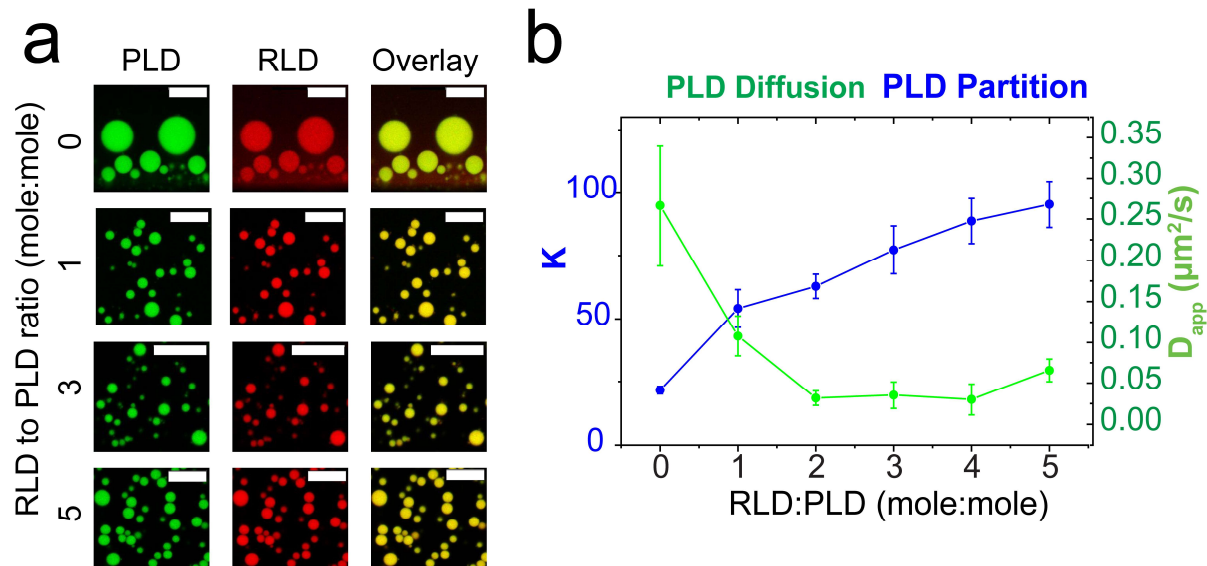


Figure S3. FUS^{PLD} partition and apparent diffusion are altered with increasing RLD concentration. (a) Multicolor confocal fluorescence microscopy images for PLD-RLD condensates at a variable RLD-to-PLD mixing ratio. For all samples, PLD concentration is fixed at 280 μM and RLD ([RGRGG]₅) concentration was varied. Scale bars represent 20 μm . ~500 nM Alexa488-labeled PLD and ~500 nM Alexa594-labeled [RGRGG]₅ were used for visualization. (b) A plot showing PLD partition coefficient (K) and apparent diffusion coefficient (D_{app}) as a function of RLD-to-PLD mixing ratio. Error bars represent ± 1 s.d. (see the statistical analysis section and Fig. 1b&c, maintext). The sample buffer contains 25 mM Tris-HCl (pH 7.5), 150 mM NaCl and 20 mM DTT.

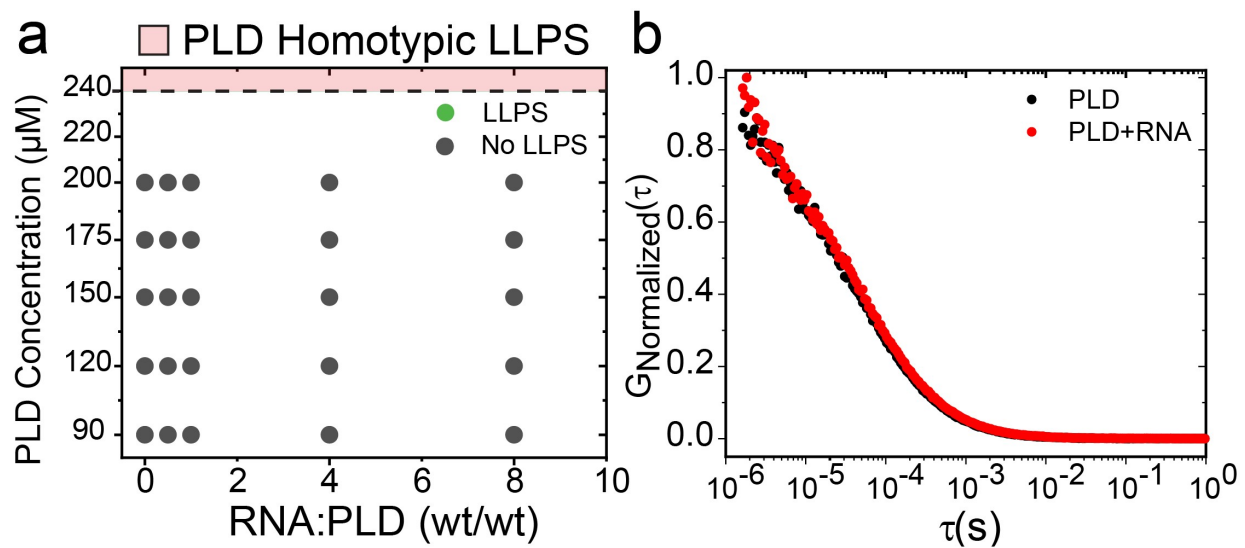


Figure S4. State diagram analysis and Fluorescence Correlation Spectroscopy (FCS) for PLD-RNA mixture. (a) State diagram of PLD-RNA mixtures, showing that poly(U) RNA has no effect on PLD phase-separation. Shaded pink region denotes PLD homotypic phase separation regime (PLD saturation concentration: $C_{\text{sat}} \sim 240 \mu\text{M}$). (b) Normalized auto-correlation curve for FUS^{PLD} in the presence (red) and absence of RNA (black). The time scale at which the autocorrelation reaches zero is proportional to the diffusion time of the labeled molecules. PLD shows identical auto-correlation time-scale both in the presence and absence of RNA, indicating that PLD is not forming a complex with RNA (which would slow the diffusion and therefore would change the autocorrelation timescale). The sample contained [Alexa488-labeled FUS^{PLD}] = 50 nM (0.88 ng/ml) with 0.0 ng/ml RNA poly(U) (black) and 7.1 ng/ml RNA poly(U) (red). The sample buffer contains 25 mM Tris-HCl (pH 7.5), 150 mM NaCl.

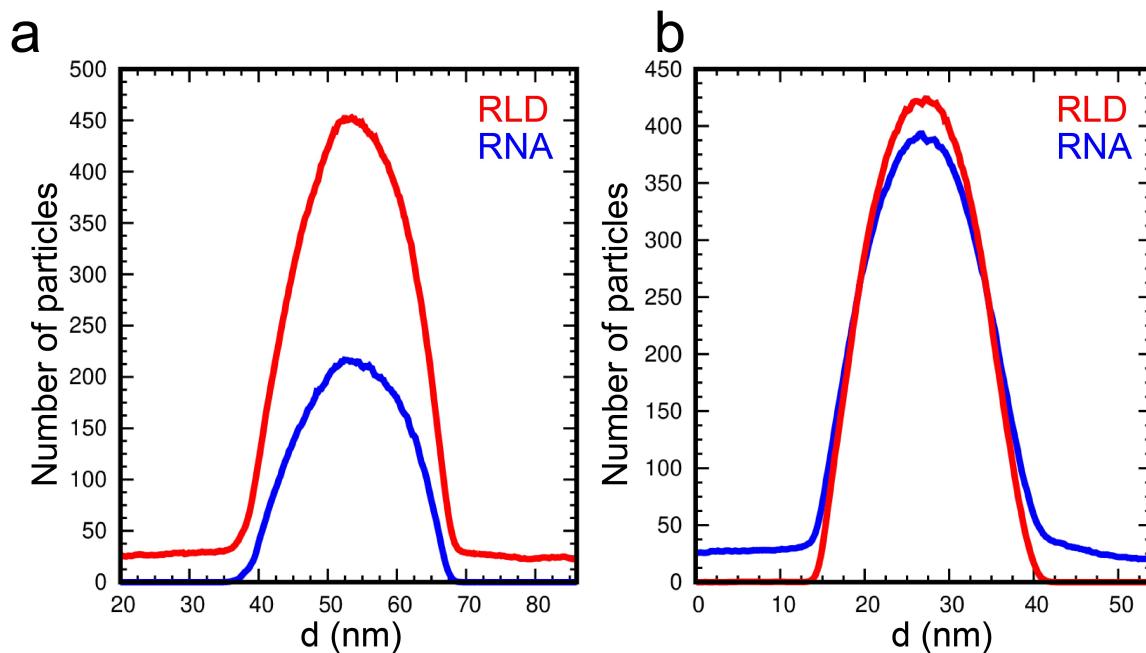


Fig. S5. Density profiles of RNA and RLD from MD simulations. Density profiles for the RLD (FUS^{RGG3}) and poly(U) RNA across RLD-RNA condensates from MD simulations at **(a)** $C_{RNA} < C_{RLD}$ **(b)** and $C_{RNA} > C_{RLD}$. These profiles correspond to the MD configurations shown in Figure 1d in the maintext. For both simulations, $C_{RLD} = 1.3$ mg/ml and the RNA-to-RLD (wt/wt) ratio is 0.5 for (a) and 1.7 for (b).

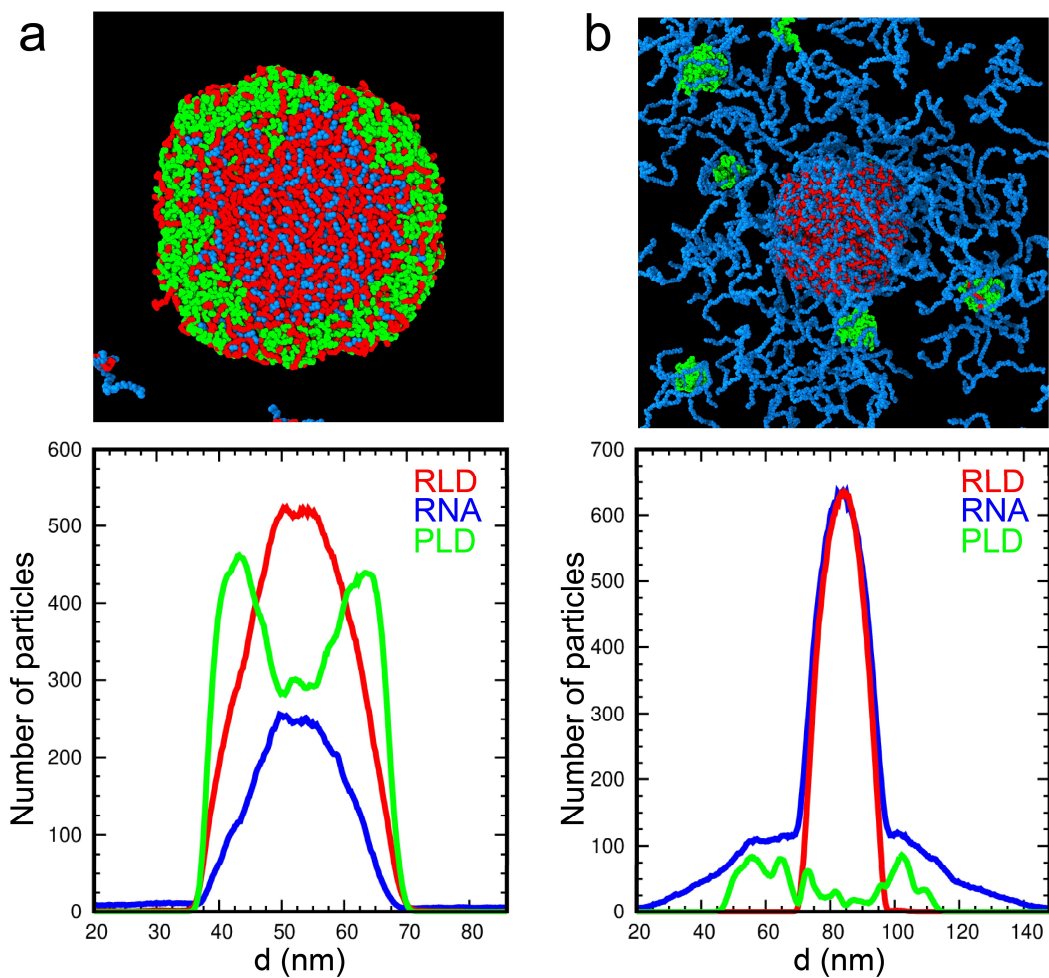


Fig. S6. Density profiles of RNA, RLD, and PLD from MD simulations. Equilibrium configurations from MD simulations and the corresponding density profiles for the RLD (FUS^{RGG3}), PLD (FUS^{PLD}) and poly(U) RNA across RLD-RNA condensates at **(a)** $C_{\text{RNA}} < C_{\text{RLD}}$ and **(b)** $C_{\text{RNA}} > C_{\text{RLD}}$. The recruitment of PLD is enhanced at $C_{\text{RNA}} < C_{\text{RLD}}$ with a visible localization of PLD chains on the surface of the RLD-RNA condensates. For both simulations, $C_{\text{RLD}} = 1.3$ mg/ml, $C_{\text{PLD}} = 0.4$ mg/ml and the RNA-to-RLD ratio (wt/wt) is 0.5 for (a) and 1.7 for (b).

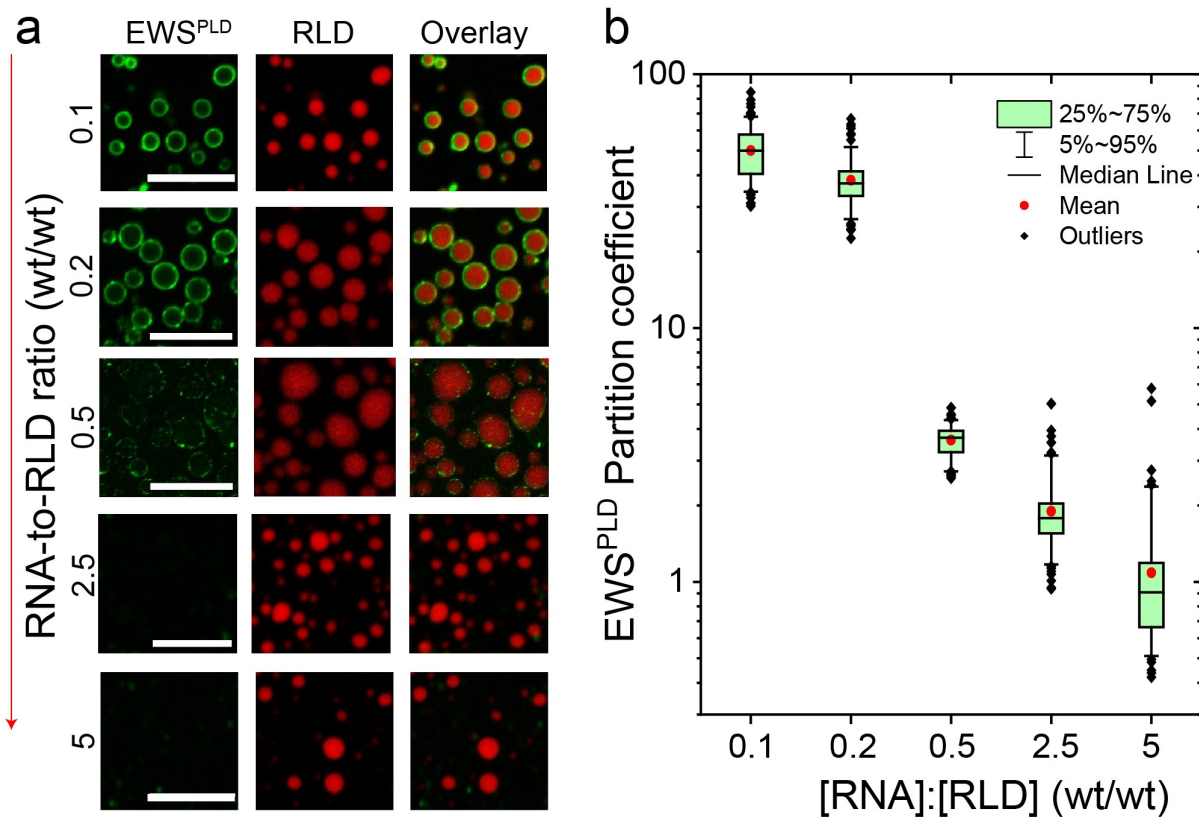


Figure S7. EWS^{PLD} preferentially partitions into the surface of RLD-rich RLD-RNA condensates. Multicolor confocal fluorescence microscopy images (**a**) and partition coefficients box plot (**b**) showing that EWS^{PLD} (labeled with Alexa488) is recruited into RNA-RLD [poly(U)-FUS^{RGG3}] droplets at low RNA-to-RLD ratio while at high RNA-to-RLD ratio, PLD partitioning significantly decreases. poly(U)-FUS^{RGG3} condensates were prepared at FUS^{RGG3}=1 mg/ml (with ~ 1% Alexa594-labeled peptide) and varying poly(U)-to-FUS^{RGG3} ratio. The number of droplets (n) analyzed across different samples for partition is n ≥ 100. Scale bars represent 10 μm. The sample buffer contains 25 mM Tris-HCl (pH 7.5), 150 mM NaCl and 20 mM DTT.

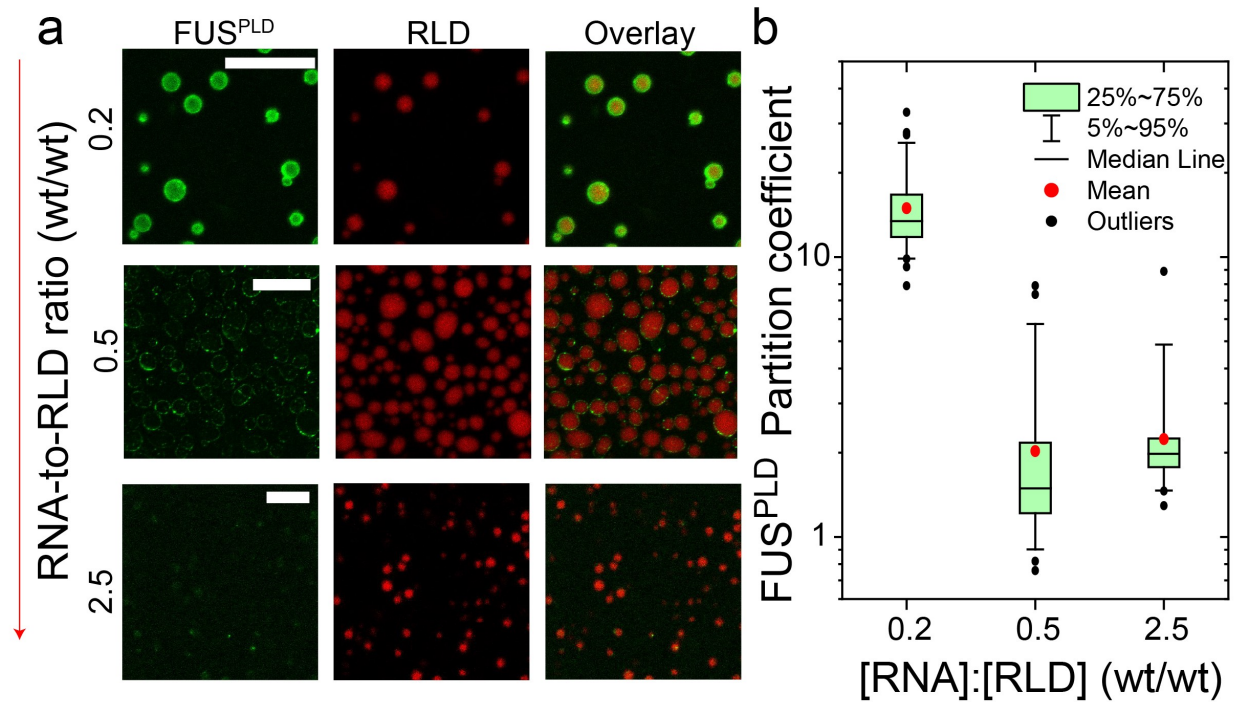


Figure S8. FUS^{PLD} shows preferential partitioning into RLD-rich RLD-RNA condensates. Multicolor confocal fluorescence microscopy images (**a**) and partition coefficient box plot (**b**) showing that FUS^{PLD} is recruited into RNA-RLD [poly(U)-FUS^{RGG3}] droplets at low RNA-to-RLD ratio while at high RNA-to-RLD, PLD (labeled with Alexa488) partitioning significantly decreases. poly(U)-FUS^{RGG3} condensates were prepared at FUS^{RGG3} = 1 mg/ml (with ~ 1% labeled:unlabeled ratio of Alexa594-FUS^{RGG3}) and varying poly(U)-to-FUS^{RGG3} ratio. The number of droplets (n) analyzed across different samples for partition coefficient calculation was kept at n ≥ 50. Scale bars represent 10 μm. The sample buffer contains 25 mM Tris-HCl (pH 7.5), 150 mM NaCl and 20 mM DTT.

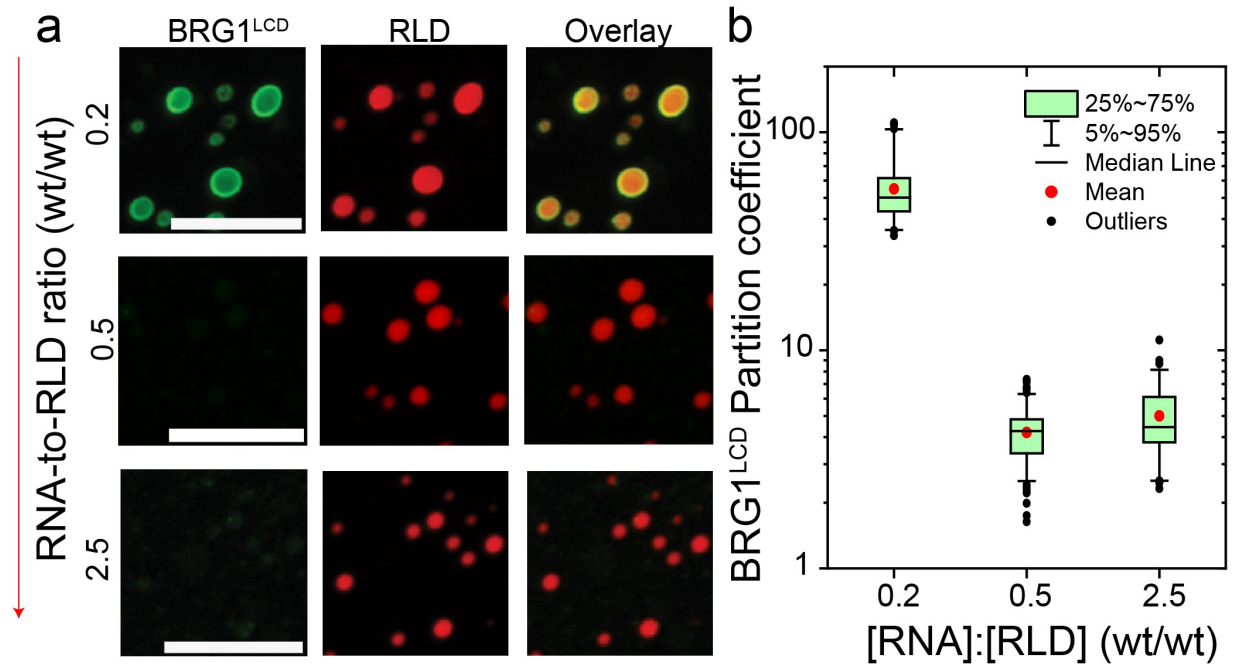


Figure S9. BRG1^{LCD} shows preferential partitioning into RLD-rich RLD-RNA condensates. Multicolor confocal fluorescence microscopy images (**a**) and partition coefficient box plot (**b**) showing that BRG1^{LCD} is recruited into RNA-RLD [poly(U)-FUS^{RGG3}] droplets at low RNA-to-RLD ratio while at high RNA-to-RLD, PLD (labeled with Alexa488) does not show any preferential partitioning. Poly(U)-FUS^{RGG3} condensates were prepared at FUS^{RGG3}=1 mg/ml (with ~ 1% labeled:unlabeled Alexa594-FUS^{RGG3}) and varying poly(U)-to-FUS^{RGG3} ratio. The number of droplets (n) analyzed across different samples for partition coefficient calculation was kept at n ≥ 75. Scale bars represent 10 μm. The sample buffer contains 25 mM Tris-HCl (pH 7.5), 150 mM NaCl and 20 mM DTT.

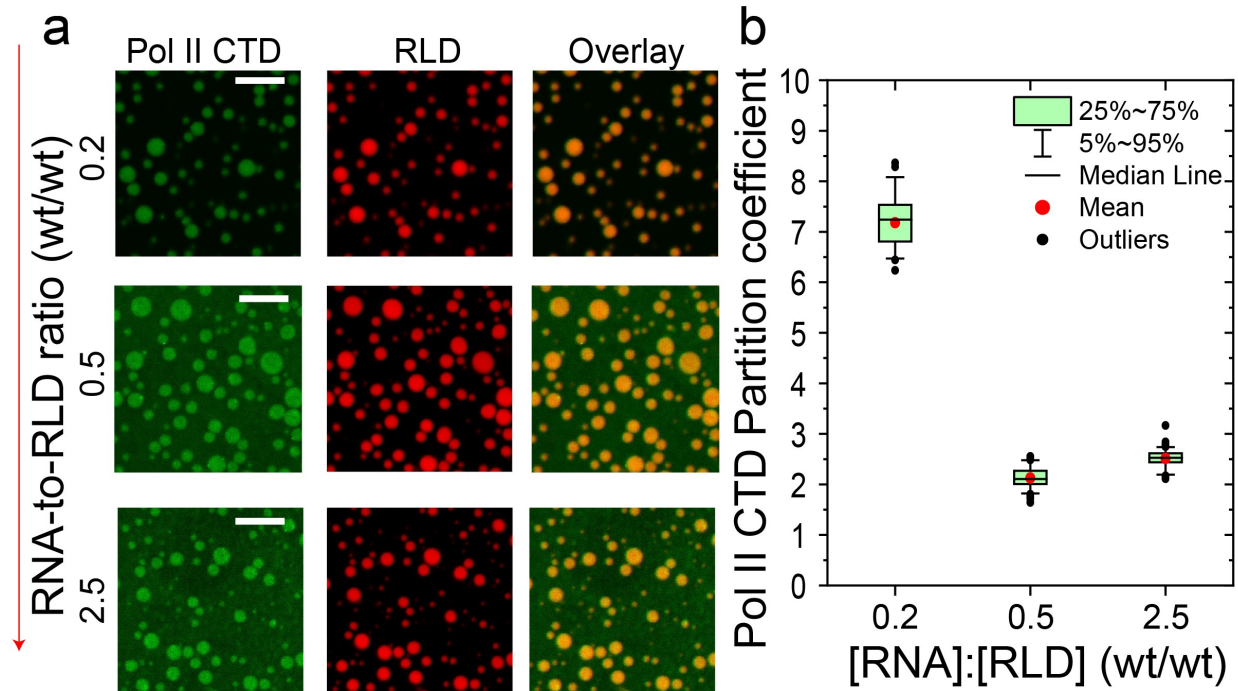


Figure S10. RNA Pol II CTD preferentially partitions into RLD-rich RLD-RNA condensates. Multicolor confocal fluorescence microscopy images (**a**) and partition coefficients box plot (**b**) showing that Pol II CTD (labeled with Alexa488) is recruited into RLD-RNA [poly(U)-FUS^{RGG3}] droplets at low RNA-to-RLD ratio while at high RNA-to-RLD, Pol II CTD shows relatively lower partitioning. poly(U)-FUS^{RGG3} condensates were prepared at FUS^{RGG3} = 1 mg/ml (with ~1% labeled:unlabeled Alexa594-FUS^{RGG3}) and varying poly(U)-to-FUS^{RGG3} ratio, as indicated. The number of droplets (n) analyzed across different samples for partition coefficient calculation was kept at n ≥ 45. Scale bars represent 10 μm. The sample buffer contains 25 mM Tris-HCl (pH 7.5), 150 mM NaCl and 20 mM DTT.

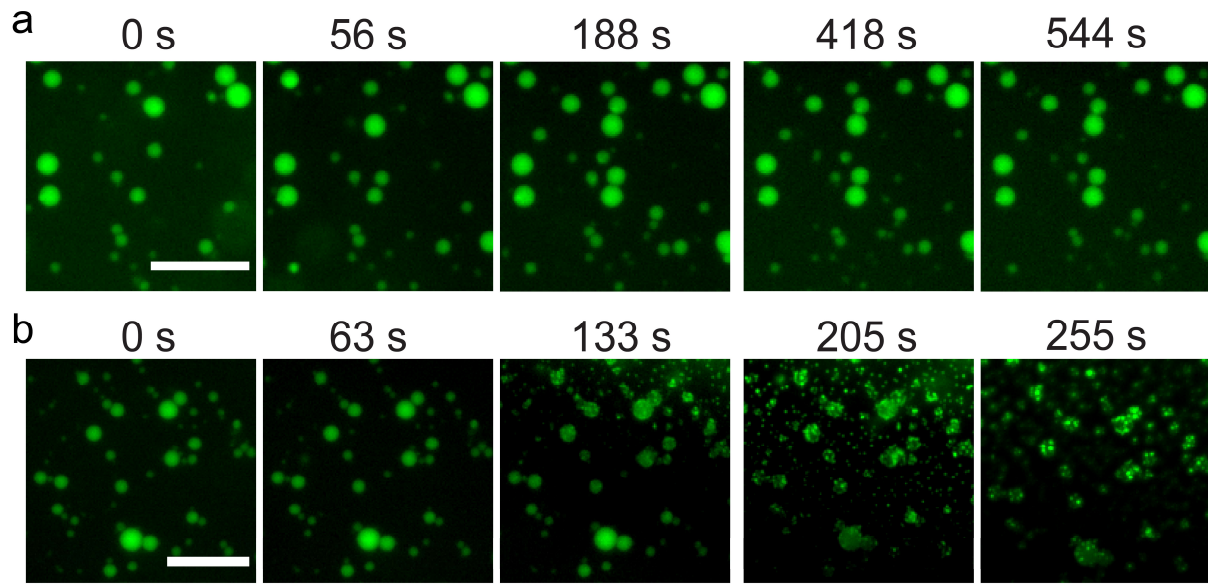


Figure S11. RNA mediated PLD-RLD demixing behavior is not impacted by sample volume change. (a) Time-lapse microscopy images after the addition of buffer to a sample containing PLD-RLD condensates showing the PLD-RLD droplets are not affected by the volume change. The sample was prepared at $[FUS^{PLD}] = 250 \mu\text{M}$ and $[FUS^{RGG3}] = 750 \mu\text{M}$ (2.6 mg/ml). $1 \mu\text{L}$ of buffer was added to the $4 \mu\text{L}$ droplet sample. (b) Time-lapse microscopy images after the addition of poly(U) RNA to a sample containing PLD-RLD condensates showing the sequestering of RLD (i.e. FUS^{RGG3}) from the PLD-RLD droplets. The sample was prepared at identical concentrations to those shown in (a). $0.3 \mu\text{L}$ of poly(U) stock solution was added to the $4 \mu\text{L}$ droplet sample, resulting in 6.5 mg/ml final concentration of poly(U) RNA. $\sim 500 \text{ nM}$ Alexa488-labeled FUS^{RGG3} was used for imaging. Scale bar = $20 \mu\text{m}$. The sample buffer contains 25 mM Tris-HCl (pH 7.5), 150 mM NaCl and 20 mM DTT.

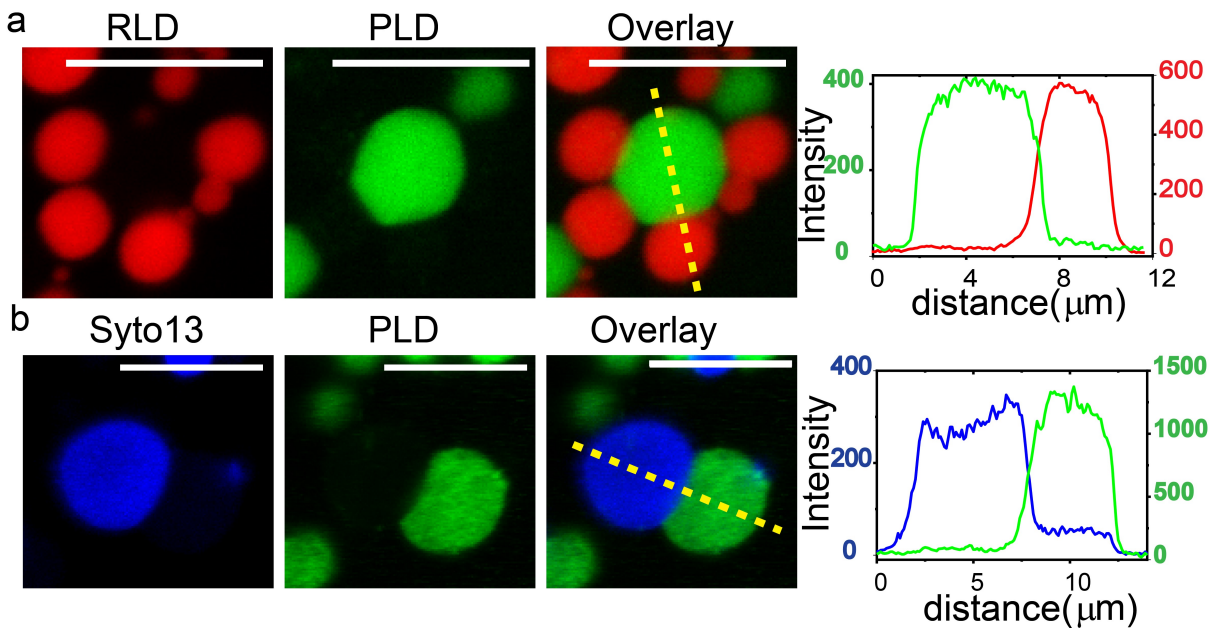


Figure S12. PLD condensates' coexistence with RLD-RNA condensates. (a) Multicolor confocal fluorescence microscopy images and intensity profiles for co-existing homotypic FUS^{PLD} droplets and heterotypic RLD-RNA droplets. PLD droplets (prepared at [FUS^{PLD}] = 400 μM) are mixed with RLD-RNA droplets (prepared at [RGRGG]₅ = 4 mg/ml and [poly(U)] = 10 mg/ml). For imaging, ~ 500 nM Alexa594-labeled [RGRGG]₅ and ~500 nM Alexa488-labeled FUS^{PLD} were used. Scale bars represent 10 μm. (b) Identical sample with RNA stained by SYTO13 nucleic acid-staining dye (for imaging FUS^{PLD} here, Cy5-labeled protein was used). Scale bars represent 8 μm. The sample buffer contains 25 mM Tris-HCl (pH 7.5), 150 mM NaCl and 20 mM DTT.

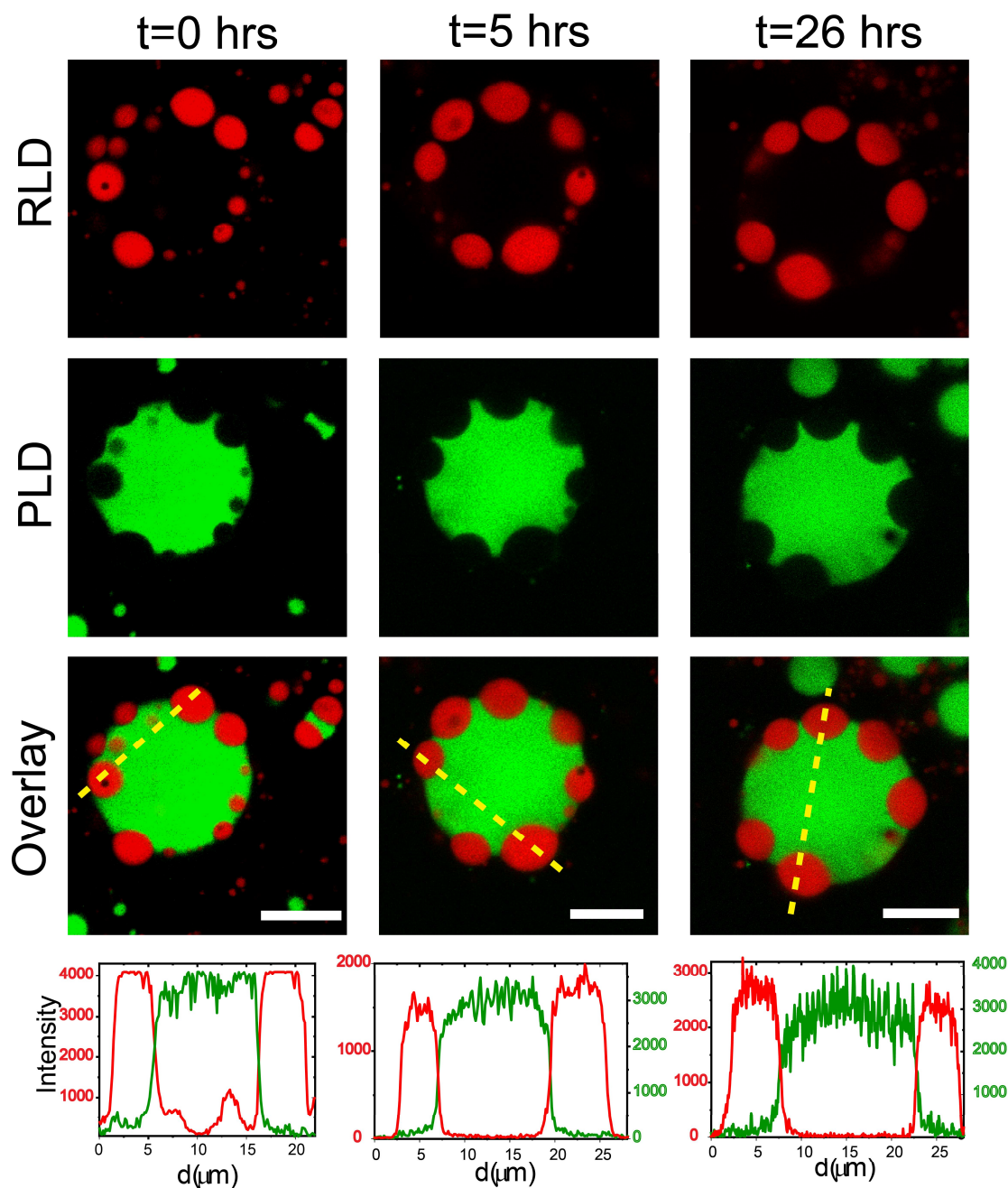


Figure S13. Stability of multi-phasic PLD-RLD-RNA condensates. Multicolor confocal fluorescence time-lapse images and intensity profiles for co-existing homotypic PLD droplets and heterotypic RLD-RNA droplets. The sample was prepared at $[FUS^{PLD}] = 400 \mu\text{M}$, $[RGRGG]_5 = 2 \text{ mg/ml}$ and $[\text{poly(U)}] = 5 \text{ mg/ml}$. For imaging, 500 nM Alexa594-labeled $[RGRGG]_5$ and 500 nM Alexa488-labeled FUS^{PLD} were used. Scale bar represents $10 \mu\text{m}$. The sample buffer contains 25 mM Tris-HCl (pH 7.5), 150 mM NaCl and 20 mM DTT.

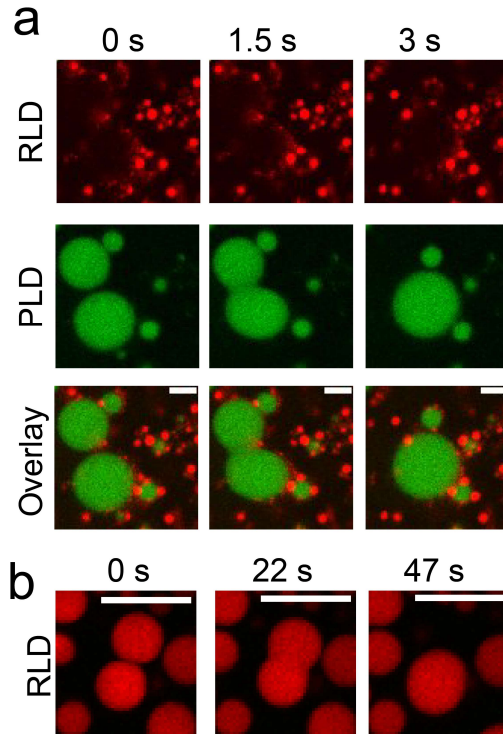


Figure S14. RLD-RNA condensates and PLD condensates show coalescence behavior. Multicolor confocal fluorescence time-lapse images showing the coalescence of **(a)** FUS^{PLD} condensates and **(b)** RLD (FUS^{RGG3})-RNA condensates in a PLD-RLD-RNA ternary mixture. For the data in **(a)**, the sample was prepared at [FUS^{PLD}]=250 μ M, [FUS^{RGG3}]=750 μ M (2.6 mg/ml) and [poly(U)]=13.0 mg/ml. 500 nM Alexa488-labeled PLD and 500 nM Alexa594-labeled RLD were used for visualization. Scale bar represents 5 μ m. For the data in **(b)**, The sample was prepared at [FUS^{PLD}] = 250 μ M, [FUS^{RGG3}] = 750 μ M (2.6 mg/ml) and [poly(A)] = 6.5 mg/ml. Scale bar represents 8 μ m. Both samples were prepared in a 25 mM Tris-HCl (pH 7.5), 150 mM NaCl and 20 mM DTT buffer.

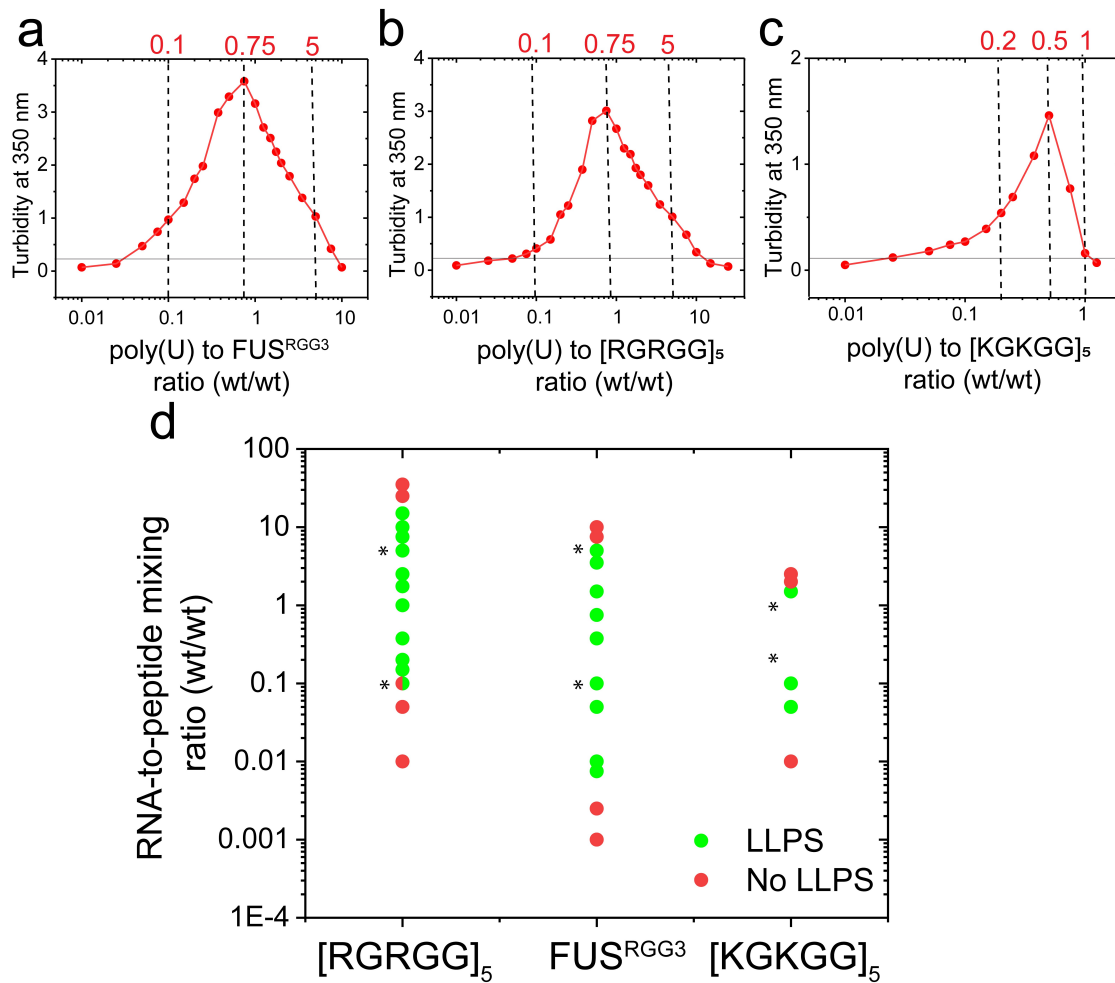


Figure S15. RLD and KLD undergo reentrant condensation with RNA. (a) Turbidity at 350 nm for FUS^{RGG3}-poly(U) mixtures prepared at FUS^{RGG3} concentration of 0.347 mg/ml and variable poly(U) RNA concentrations. (b) Replotting² of the turbidity at 350 nm for [RGRGG]₅-poly(U) mixtures prepared at [RGRGG]₅ concentration of 0.24 mg/ml and variable poly(U) RNA concentrations. (c) Replotting² of the turbidity at 350 nm for [KGKGG]₅-poly(U) mixtures prepared at [KGKGG]₅ concentration of 0.22 mg/ml and variable poly(U) RNA concentrations. (d) Phase strips² of peptide-RNA mixtures. For each strip, the peptide concentration was fixed at 0.24, 0.3, and 0.22 mg/ml for [RGRGG]₅, FUS^{RGG3}, and [KGKGG]₅, respectively. poly(U) RNA concentration was varied. The sample phase separation state (LLPS or no LLPS) was determined via optical microscopy. The asterisks represent the minimum and maximum mixing ratios used for the various experiments. [RGRGG]₅ and [KGKGG]₅ samples were prepared in a buffer containing 25 mM Tris-HCl (pH 7.5) and 20 mM DTT. FUS^{RGG3} samples were prepared in a buffer containing 25 mM Tris-HCl (pH 7.5), 150 mM NaCl and 20 mM DTT.

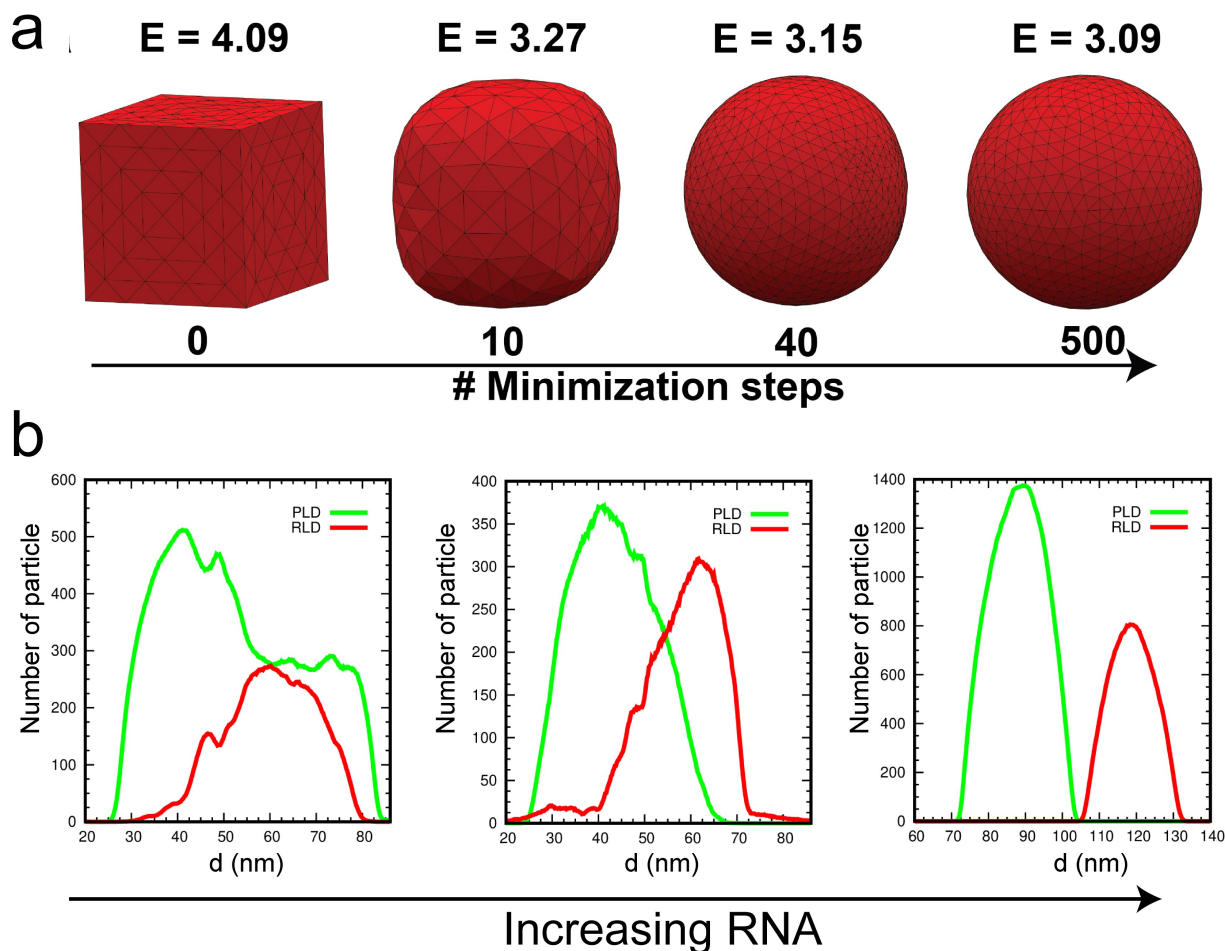


Figure S16. A simple illustration of the fluid-interface modeling simulation and density profiles for MD simulations. (a) Time evolution of a cube of liquid with 50 mN/m surface tension using Surface Evolver. The minimization of interfacial energy leads to the transition from a cube to a spherical droplet, which is the geometry with the least surface energy. **(b)** Density profiles for the molecular dynamics simulation snapshots shown in **Figure 4f** in the main-text. For simulation details, see the legend of **figure 4f** in the main-text.

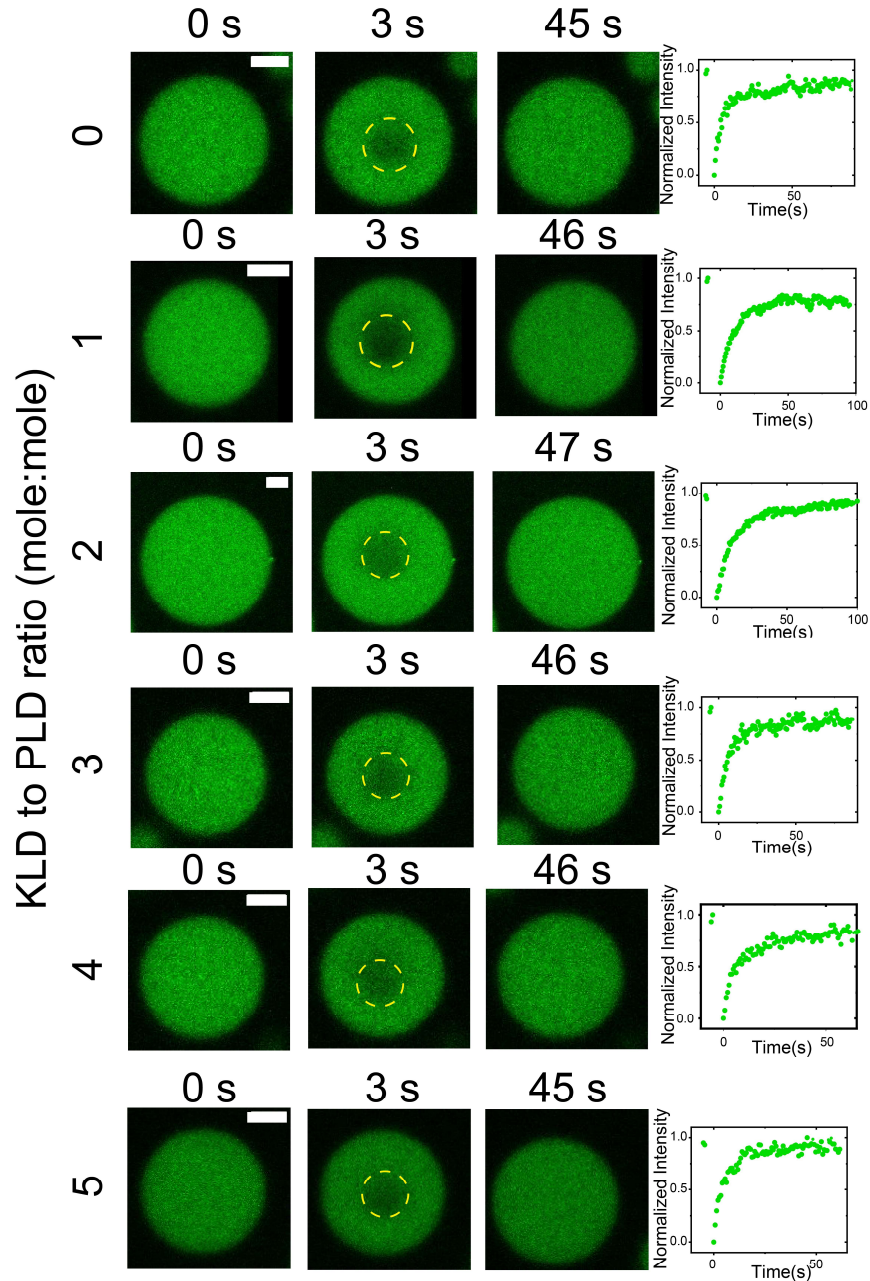


Figure S17. Representative FRAP images and intensity time traces for PLD-KLD condensates. Time-lapse FRAP images (left) and intensity time traces (right) for PLD-KLD condensates prepared at a fixed PLD concentration and variable KLD ([KKG₅]) to PLD ratio. For all samples, FUS^{PLD} concentration is fixed at 280 μ M. The sample buffer contains 25 mM Tris-HCl (pH 7.5), 150 mM NaCl and 20 mM DTT. Scale bars represent 5 μ m. Bleaching occurs at t=3s. The imaging/FRAP assay was performed utilizing ~1% Alexa488-labeled PLD (labeled:unlabeled ratio).

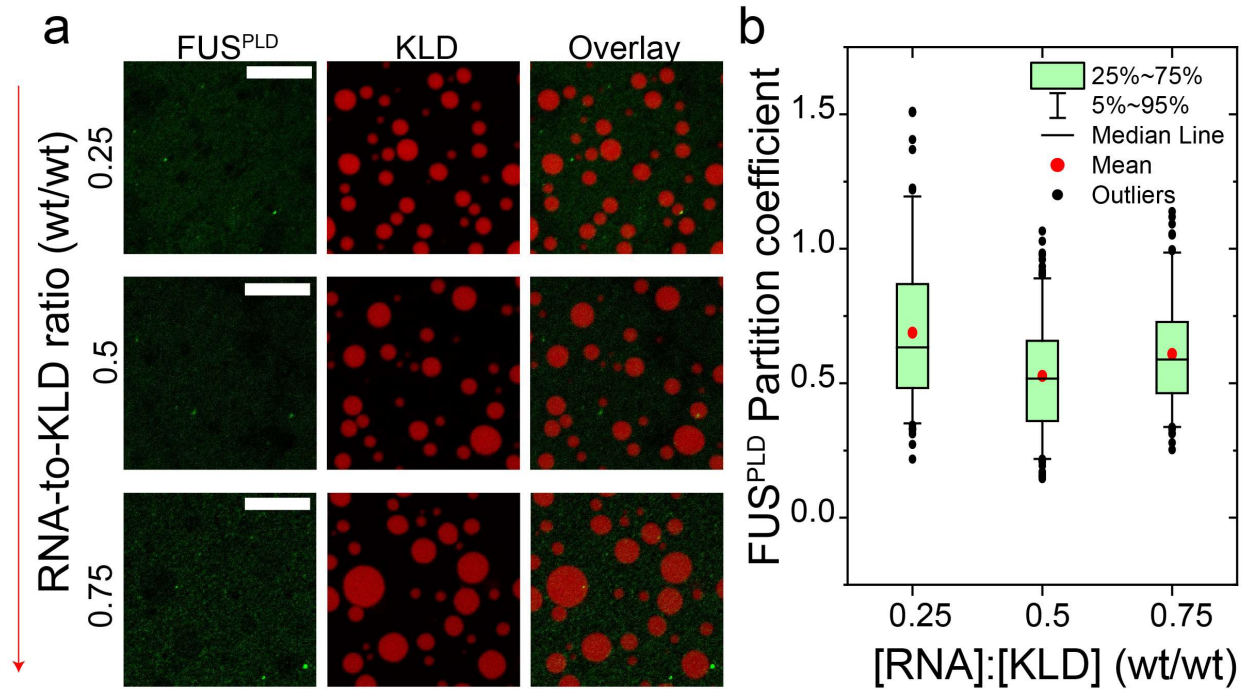


Figure S18. PLD does not partition into KLD-RNA condensates across all mixture compositions. Multicolor confocal fluorescence microscopy images and partition coefficient box plot of Alexa488-labeled FUS^{PLD} in KLD-RNA droplets. KLD-RNA condensates were prepared at fixed KLD ([KGKGG]₅) concentration of 1 mg/ml and variable RNA [poly(U)] to KLD ratio, as indicated. Scale bars represent 10 μ m. The number of droplets (n) analyzed across different samples for partition is $n \geq 150$. The sample buffer contains 25 mM Tris-HCl (pH 7.5), 150 mM NaCl and 20 mM DTT.

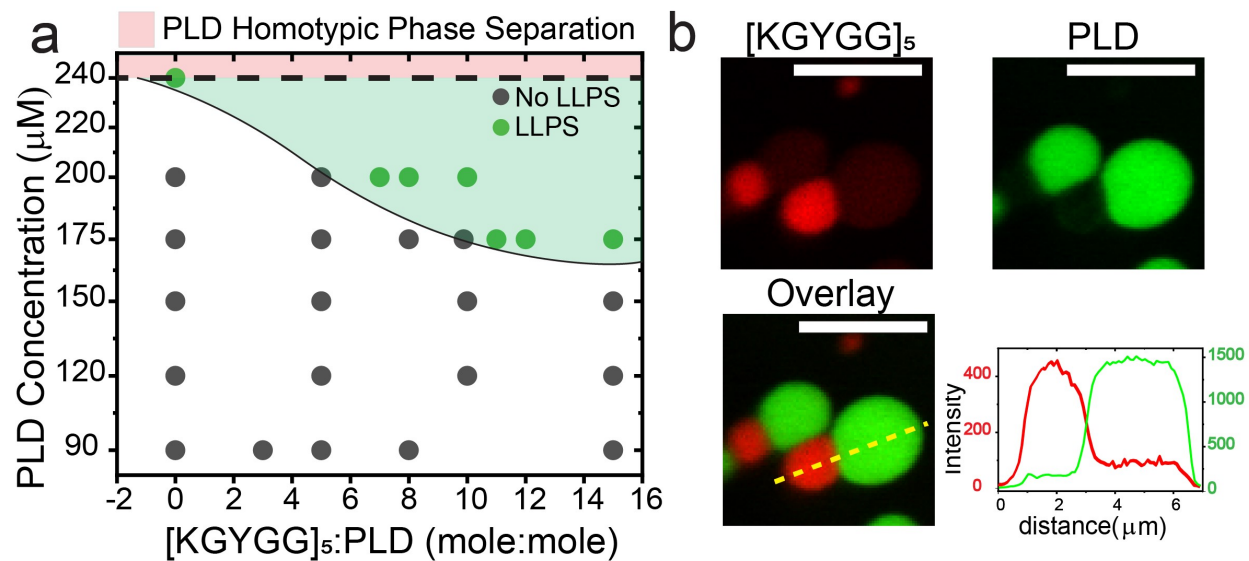


Figure S19. A tyrosine-variant of KLD restores PLD binding ability and stabilizes a shared fluid-fluid interface. (a) Isothermal state diagram of FUS^{PLD}-[KGYGG]₅ mixtures showing that [KGYGG]₅ facilitates PLD phase-separation. The shaded green region shows the heterotypic phase separation regime for PLD-[KGYGG]₅ mixtures while the shaded pink region denotes the PLD homotypic phase separation regime (saturation concentration $\sim 240 \mu\text{M}$). Both shaded regions are drawn as a guide to the eye. All samples were prepared in a 25 mM Tris-HCl, 150 mM NaCl and 20 mM DTT buffer. (b) Multicolor confocal fluorescence microscopy images and intensity profiles for co-existing homotypic FUS^{PLD} droplets and heterotypic [KGYGG]₅-RNA droplets. Each type of droplets were separately prepared at initial concentrations of [FUS^{PLD}]=400 μM , [KGYGG]₅=4 mg/ml and [poly(U)]=0.4 mg/ml and then mixed (1:1 vol/vol). For imaging, 1% Alexa594-labeled [KGYGG]₅ and Alexa488-labeled FUS^{PLD} were used (labeled:unlabeled ratio). Scale bar represents 5 μm .

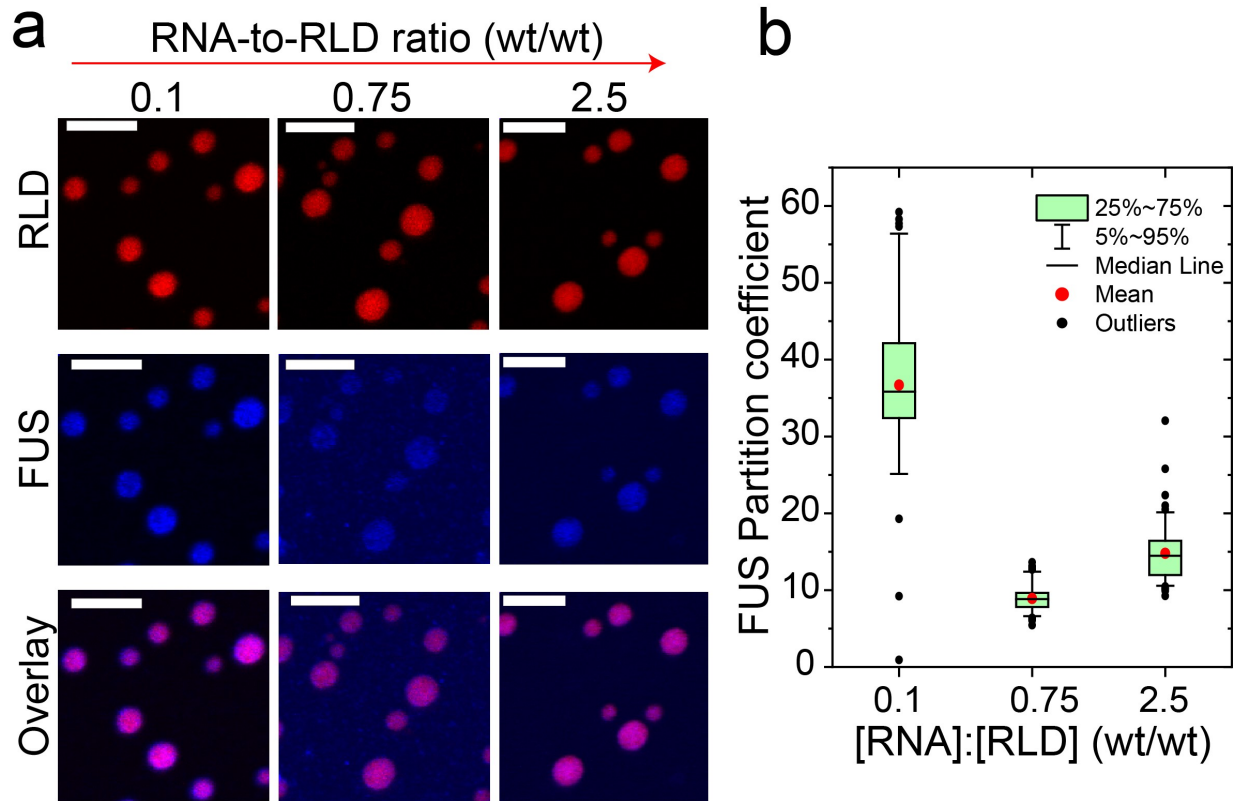


Figure S20. Full-length FUS (FUS^{FL}) partitions into RLD-RNA condensates across all mixture compositions. Multicolor confocal fluorescence microscopy images (**a**) and partition coefficient box plot (**b**) showing the partition of FUS^{FL} (labeled with Alexa488) in RNA-RLD droplets at varying RNA-to-RLD ratio. RNA-RLD condensates were prepared at FUS^{RGG3}=1 mg/ml (labeled with Alexa594) and varying RNA [poly(U)] to FUS^{RGG3} ratio. The number of droplets (n) analyzed across different samples for partition is n ≥ 80. Scale bars represent 5 μm. The samples were prepared in a buffer containing 25 mM Tris-HCl (pH 7.5), 150 mM NaCl, and 20 mM DTT. Compare this data with Figure 1h&k in the main-text.

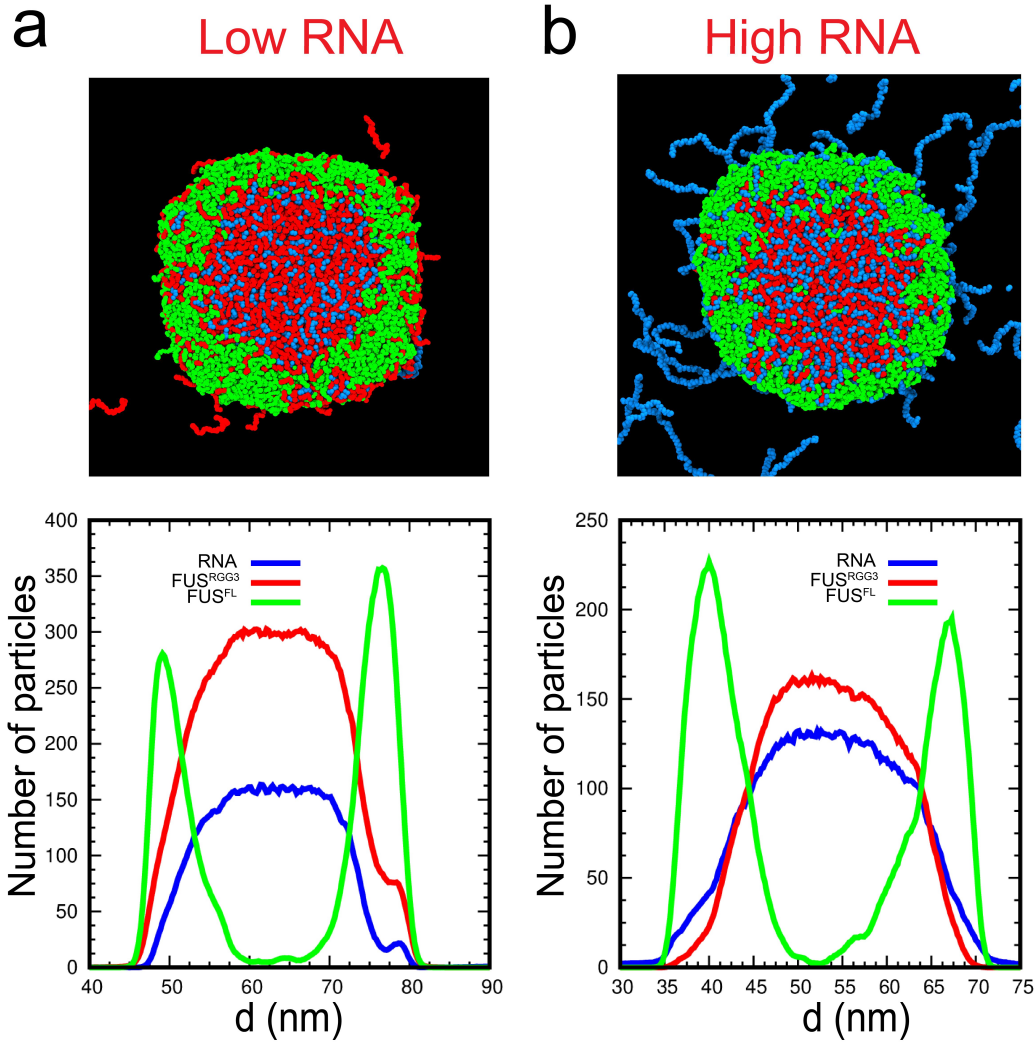


Figure S21. Molecular dynamics simulation snapshots showing the partition of FUS^{FL} in RLD-RNA droplets. Representative equilibrium configurations and corresponding density profiles obtained from molecular dynamics simulation of RLD-RNA condensates at both low (**a**) and high (**b**) RNA-to-RLD mixing ratios. FUS^{FL} accumulates at the surface of RLD-RNA condensates in both conditions due to its ability to interact with RLD chains (through PLD-RLD interactions) and RNA chains (through RBD-RNA interactions, see Fig. 5e, main-text). RNA is visualized as blue chains, RLD is visualized as red chains, and FUS^{FL} is visualized as green chains. For both simulations, $C_{RLD}=1.3$ mg/ml, $C_{FUS}=0.7$ mg/ml and RNA-to-RLD ratio (wt/wt) of 0.5 (left) and 2.0 (right).

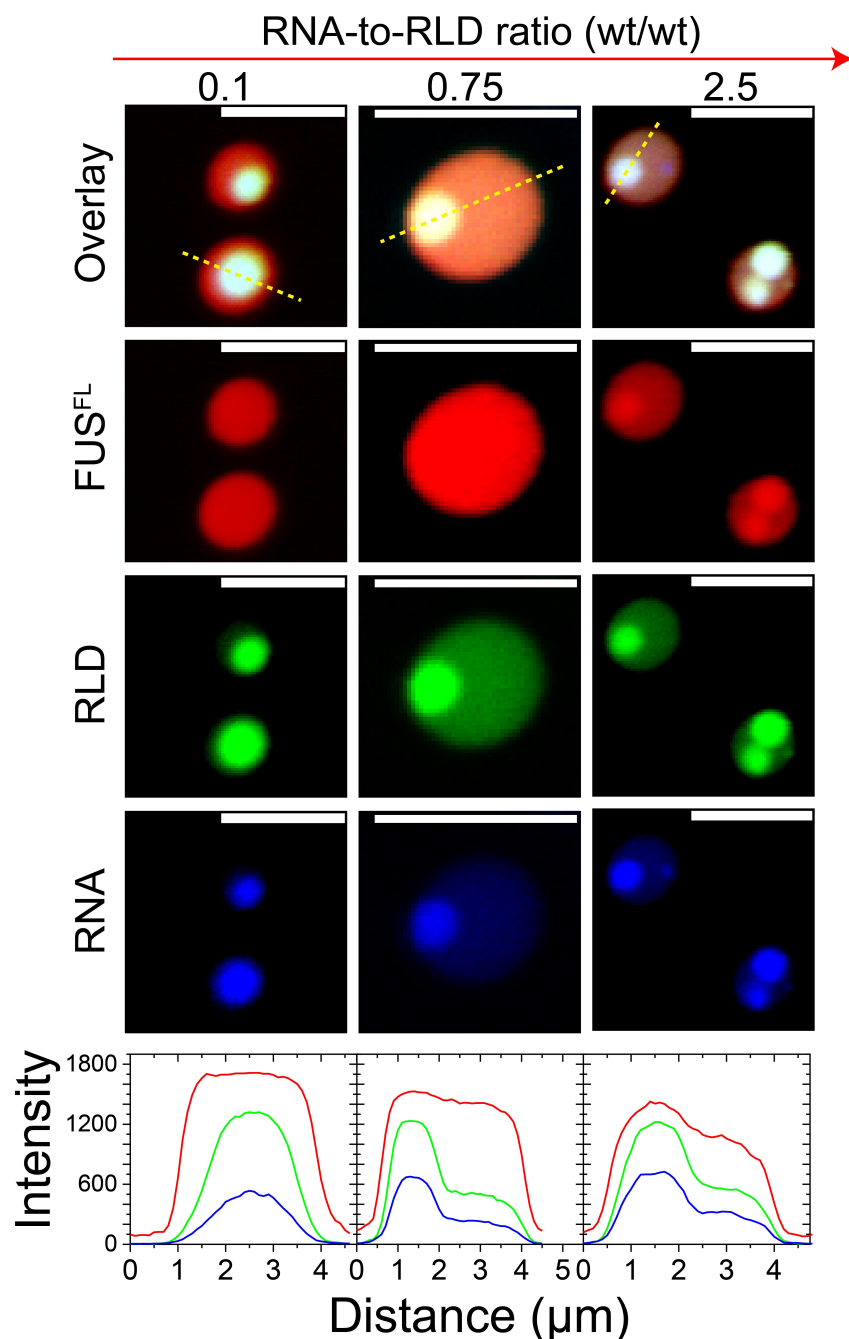


Figure S22. FUS^{FL} condensates completely engulf RLD-RNA condensates across all mixture compositions. Multicolor confocal fluorescence microscopy images and intensity profiles for co-existing homotypic FUS^{FL} droplets (red; Cy5-labeled FUS^{PLD}) and heterotypic RLD (green; Alexa594-labeled FUS^{RGG3}) and poly(U) RNA (blue; probed by SYTO13) condensates at different RNA-to-RLD ratio. Each type of droplets was separately prepared at [FUS^{FL}]= 21.3 μM, [FUS^{RGG3}] = 1 mg/ml and varying RNA-to-RLD ratios, as indicated, and then mixed (1:1 vol/vol). All samples were made in a buffer containing 25 mM Tris-HCl (pH 7.5), 150 mM NaCl, and 20 mM DTT. All fluorescent probes were added at a 1% labeled:unlabeled ratio. All scale bars represent 5 μm.

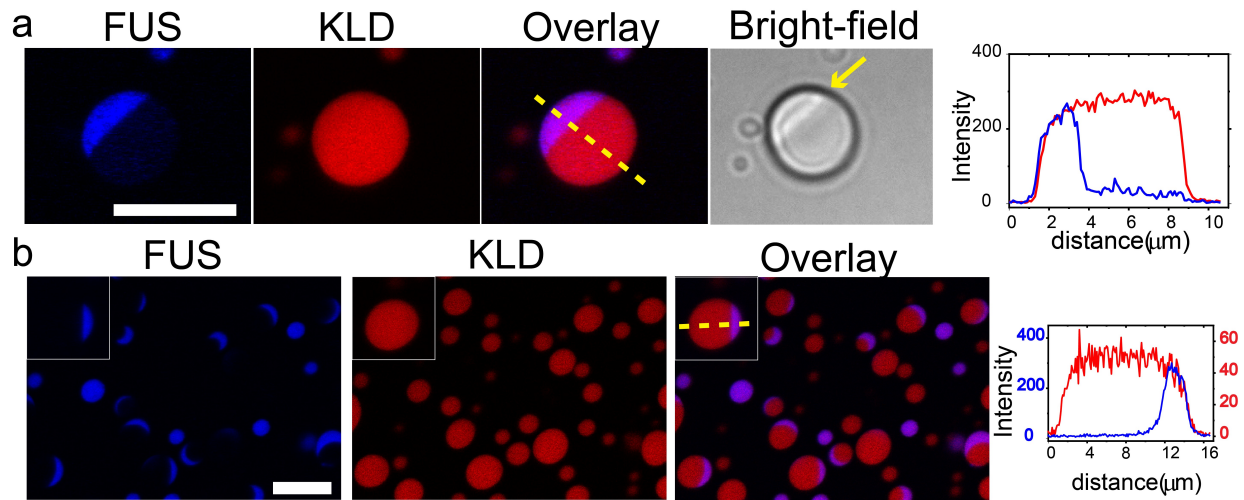


Figure S23. Janus-like architecture of FUS-KLD-RNA condensates. Multicolor confocal fluorescence and bright-field microscopy images and intensity profiles for Janus droplets formed by homotypic FUS droplets (*blue*) and heterotypic KLD-RNA condensates (*red*). Each type of droplets were separately prepared at initial concentrations of $[FUS^{FL}] = 22 \mu\text{M}$, $[KGKGG]_5 = 4 \text{ mg/ml}$ and RNA $[\text{poly(U)}] = 3 \text{ mg/ml}$ keeping $[KGKGG]_5$ to poly(U) ratio at 0.75 (wt/wt) and then mixed (1:1 vol/vol). For imaging, 500 nM Alexa594-labeled $[KGKGG]_5$, 500 nM Alexa488-labeled FUS^{FL} were used for (a); and 500 nM Alexa594-labeled $[KGKGG]_5$, 500 nM Alexa488-labeled FUS^{PLD} were used for (b). The arrow in (a) points to the line separating the two lobes of the Janus droplet (visible in the bright-field channel). All samples were prepared in a buffer containing 25 mM Tris-HCl (pH 7.5), 150 mM NaCl, and 20 mM DTT. Scale bar represents 10 μm . Inset shows the zoomed-in appearance of a Janus droplet.

Supplementary Movie Legends

Movie S1. Multicolor fluorescence microscopy video showing that the addition of poly(U) RNA induces condensate switching effect wherein PLD-RLD condensates transition to RLD-RNA condensates. (PLD: green, RLD: red). Scale bar is 20 μm .

Movie S2. Multicolor fluorescence microscopy video showing that the addition of poly(U) RNA causes the demixing of PLD and RLD from well-mixed PLD-RLD condensates to coexisting PLD homotypic condensates and RLD-RNA heterotypic condensates. (PLD: green, RLD: red). Scale bar is 10 μm .

References

- 1 Kaur, T. *et al.* Molecular crowding tunes material states of ribonucleoprotein condensates. *Biomolecules* **9**, 71 (2019).
- 2 Alshareedah, I. *et al.* Interplay between Short-Range Attraction and Long-Range Repulsion Controls Reentrant Liquid Condensation of Ribonucleoprotein–RNA Complexes. *Journal of the American Chemical Society* **141**, 14593-14602, doi:10.1021/jacs.9b03689 (2019).
- 3 Banerjee, P. R., Moosa, M. M. & Deniz, A. A. Two-Dimensional Crowding Uncovers a Hidden Conformation of α -Synuclein. *Angewandte Chemie* **128**, 12981-12984 (2016).
- 4 Banerjee, P. R. & Deniz, A. A. Shedding light on protein folding landscapes by single-molecule fluorescence. *Chemical Society Reviews* **43**, 1172-1188 (2014).
- 5 Banerjee, P. R., Milin, A. N., Moosa, M. M., Onuchic, P. L. & Deniz, A. A. Reentrant Phase Transition Drives Dynamic Substructure Formation in Ribonucleoprotein Droplets. *Angew Chem Int Ed Engl* **56**, 11354-11359, doi:10.1002/anie.201703191 (2017).
- 6 Banerjee, P. R., Mitrea, D. M., Kriwacki, R. W. & Deniz, A. A. Asymmetric Modulation of Protein Order-Disorder Transitions by Phosphorylation and Partner Binding. *Angew Chem Int Ed Engl* **55**, 1675-1679, doi:10.1002/anie.201507728 (2016).
- 7 Kang, M., Day, C. A., Kenworthy, A. K. & DiBenedetto, E. Simplified equation to extract diffusion coefficients from confocal FRAP data. *Traffic* **13**, 1589-1600, doi:10.1111/tra.12008 (2012).
- 8 Schindelin, J. *et al.* Fiji: an open-source platform for biological-image analysis. *Nature methods* **9**, 676 (2012).
- 9 Brakke, K. A. The surface evolver. *Experimental mathematics* **1**, 141-165 (1992).
- 10 Berthier, J. & Brakke, K. A. *The physics of microdroplets*. (John Wiley & Sons, 2012).
- 11 Dignon, G. L., Zheng, W., Best, R. B., Kim, Y. C. & Mittal, J. Relation between single-molecule properties and phase behavior of intrinsically disordered proteins. *Proceedings of the National Academy of Sciences* **115**, 9929-9934 (2018).
- 12 Anderson, J. A., Lorenz, C. D. & Travesset, A. General purpose molecular dynamics simulations fully implemented on graphics processing units. *Journal of computational physics* **227**, 5342-5359 (2008).
- 13 Glaser, J. *et al.* Strong scaling of general-purpose molecular dynamics simulations on GPUs. *Computer Physics Communications* **192**, 97-107 (2015).
- 14 Gasteiger, E. *et al.* in *The proteomics protocols handbook* 571-607 (Springer, 2005).